REPORT TITLE: AN INVESTIGATION INTO THE MECHANICS

OF SINGLE CRYSTAL TURBINE BLADES WITH A VIEW

TOWARDS ENHANCING GAS TURBINE EFFICIENCY

FINAL SCIENTIFIC REPORT

REPORTING PERIOD START DATE:10/01/01

REPORTING PERIOD END DATE: 3/31/05

PRINCIPAL AUTHORS: K. R. Rajagopal and I. J. Rao

DATE REPORT WAS ISSUED: May 5, 2006

DOE AWARD NUMBER: DE-FC-01NT41344

NAME AND ADDRESS OF SUBMITTING ORGANIZATION: Texas

A&M University, College Station, TX-77843

SUB-CONTRACTOR: New Jersey Institute of Technology, Newark, NJ

Disclaimer

This report was prepared as an account of work sponsored by an agency of the United States Government. Neither the United States Government nor any agency thereof, nor any of their employees, makes any warranty, express or implied, or assumes any legal liability or responsibility for the accuracy, completeness, or usefulness of any information, apparatus, product, or process disclosed, or represents that its use would not infringe privately owned rights. Reference herein to any specific commercial product, process, or service by trade name, trademark, manufacturer, or otherwise does not necessarily constitute or imply its endorsement, recommendation, or favoring by the United States Government or any agency thereof. The views and opinions of authors expressed herein do not necessarily state or reflect those of the United States Government or any agency thereof.

Abstract

The demand for increased efficiency of gas turbines used in power generation and aircraft applications has fueled research into advanced materials for gas turbine blades that can withstand higher temperatures in that they have excellent resistance to creep. The term "Superalloys" describes a group of alloys developed for applications that require high performance at elevated temperatures. Superalloys have a load bearing capacity up to 0.9 times their melting temperature. The objective of the investigation was to develop a thermodynamic model that can be used to describe the response of single crystal superalloys that takes into account the microstructure of the alloy within the context of a continuum model. Having developed the model, its efficacy was to be tested by corroborating the predictions of the model with available experimental data. Such a model was developed and it is implemented in the finite element software ABAQUS/STANDARD through a user subroutine (UMAT) so that the model can be used in realistic geometries that correspond to turbine blades.

Table of Contents

Executive Summary

The demand for increased efficiency of gas turbines used in power generation and aircraft applications has fueled research into advanced materials for gas turbine blades. Higher efficiencies are possible if turbine blades can be designed to withstand inlet temperature of the order of 2200 ^{o}C or more. At such high temperatures, it is critical to use materials that have excellent resistance to creep. The term "Superalloys" describes a group of alloys developed for applications that require high performance at elevated temperatures. Superalloys have a load bearing capacity up to 0.9 times their melting temperature. They retain their strength even after long exposure time at high temperatures and they have good low temperature ductility as well.

The objective of the investigation was to develop a rational thermodynamic model that can be used to describe the response of single crystal superalloys that takes into account the microstructure of the alloy within the context of a continuum model. Having developed the model, its efficacy was to be tested by corroborating the predictions of the model with available experimental data. Such a model was developed and it is implemented in the finite element software ABAQUS/STANDARD through a user subroutine (UMAT) so that the model can be used in realistic geometries that correspond to turbine blades.

We develop a constitutive theory within a thermodynamic setting to describe the creep of single crystal super alloys that gainfully exploits the fact that the configuration that the body would attain on the removal of the external stimuli, referred to as the ''natural configuration'', evolves, with the response of the body being elastic from these evolving natural configurations. The evolution of the natural configurations is determined by the tendency of the body to undergo a process that maximizes the rate of dissipation. Here, the elastic response is assumed to be linearly elastic with cubic symmetry associated with the body which remains the same as the configuration evolves. A form for the inelastic stored energy (the energy that is _trapped_ within dislocation networks) is utilized based on simple ideas related to the motion of the dislocations. The rate of dissipation is assumed to be proportional to the density of mobile dislocations and another term that takes into account the damage accumulation due to creep. The model developed herein is used to simulate uni-axial creep of oriented single crystal nickel-base super alloys. The predictions of the theory agree well with the available experimental data for CMSX-4.

The numerical scheme developed is implemented in UMAT to study the creep behavior of single crystal superalloys loaded along the <001> orientation. The UMAT is validated by using it to obtain the results already obtained in previous sections using the semi-inverse approach. The results obtained through the UMAT is compared with the results obtained using the semi-inverse approach and the experimental results. A comparison of strain versus time curves for loading along <001> orientation at temperatures θ = 750, 982 and 1000 ^{o}C obtained using the UMAT and the semi-inverse method and experimental results. We also make a comparison for the inelastic stored energy at temperatures θ = 750, 982 and 1000 ^{o}C. A similar comparison is made for third component of the backstress tensor as knowledge of these quantities is critical in the design of single crystal super alloy blades.

We start with a discussion of single crystal superalloys, their microstructure that needs to be reflected by the model. This is followed by a discussion of the various models that are currently in vogue to describe the response of single crystal superalloys and their inadequacy in describing the creep characteristics of the material. Next we discuss the general thermodynamic framework within which the model is to be placed and follow this with the development of the

model. The specific model that is picked is introduced next, and the response of the model along certain crystallographic directions, for the range of temperatures of technical relevance, are compared against available experimental data. We find that the model performs very well and does not have the shortcomings of the models that are in use currently.

REPORT DETAILS

1. INTRODUCTION

1.1 Microstructure of superalloys

Single crystal nickel-base superalloys have been developed for gas turbine blade applications. These alloys have superior thermal, fatigue and creep properties compared to conventional cast alloys because grain boundaries have been eliminated. Typical first generation alloys include CMSX-2, second generation alloys include CMSX-4, MC-2, TMS-63, and third generation alloys include CMSX-10 with high Re content. A typical modern superalloy (e.g. CMSX-4) for turbine blades is a single crystal, which contains particles, based on the ordered γ' L1$_2$ structure, lying in a matrix based on a disordered face-centered cubic Ni$_3$Al. The γ' phase forms remarkably regular cubes packed in a rather regular cubic array and it occupies 65–70% of the volume. The two-phase structure of a superalloy contributes essentially to its excellent creep strength at high temperatures, the phase boundaries providing obstacles to dislocation motion. The volume fraction of the γ' phase is an important factor in optimizing superalloy composition to get the best creep strength. Usually a maximum in the creep strength is reached between 70% and 80% volume fraction of γ' phase with further increase leading to a significant drop in strength (see [9]). It has been observed that in the primary stage of creep in modern superalloys, and during most of the secondary creep, plastic deformation is confined to the γ channels. The γ' particles act as impenetrable obstacles. The γ' phase has another very remarkable property. Whereas most metals and alloys, including the γ matrix, have flow stresses that decrease steadily with increasing temperature, alloys related to Ni$_3$Al, and many other alloys with the L1$_2$ structure, show flow stresses that can increase by a factor of 5 as the temperature increases from room temperature to about 650 ^{o}C [37]. The high strength of γ' is especially valuable at high temperatures. The lattice parameters of the γ matrix and the γ' precipitate are very similar, but not identical. The creep deformed microstructure and many mechanical properties depend on the lattice misfit. The presence of various alloying elements strongly affects the value of misfit. The misfit could be positive or negative depending on the particular composition of the superalloy. Moreover, the misfit changes with the kind of heat treatment the alloy is subject to and it also varies with temperature [46]. The sign of the misfit plays an important role in the evolution of microstructure as the material creeps (see [46]).

Another important microstructural property of superalloys is the ability of cubic γ' phase to transform into flat plates (''rafts'') under the influence of stress and temperature. This directional coarsening is especially important in nickel base superalloys because the morphological changes in the two phase microstructure alter the creep resistance of the material in the stress and temperature range where these alloys are used in applications such as turbine blades. It has been shown by Nabarro [38] that in the elastic regime, the thermodynamic driving force for rafting is proportional to the applied stress, to the lattice misfit and to the difference of

elastic constant of the γ and γ' phases. It has also been found that the direction of rafting depends upon the direction of loading and the sign of lattice misfit. Two types of rafting behavior in <001> oriented nickel-base single crystals have been identified.

1. Type N-rafts develop transverse to the direction of the externally applied stress.

2. Type P-rafts develop parallel to the direction of the externally applied stress.

Type N behavior is usually associated with negative misfit alloys stressed in tension, or positive misfit alloys stressed in compression. Conversely, type P behavior is associated with positive misfit alloys stressed in tension, and negative misfit alloys stressed in compression. The differences in the microstructural evolution associated with a change from positive to negative misfit are an indication that the rafting is primarily dominated by internal stresses developed due to the misfit. In fact, the $\gamma - \gamma'$ interface plays an important role in the creep property of superalloys [8]. The evolution of rafts with creep depends on the applied stress and operating temperature. At temperatures beyond 950 ^{o}C, experiments (Reed et al. [64]) suggest that rafting is complete during very early stages of creep deformation. Thus, from the modeling point of view, we can take into account, only the effect which a fully rafted microstructure confers. However, at lower temperatures, it is likely that the rafts evolve at a rate comparable with the rate of the evolution of the strain, in which case a suitable criterion for the evolution of the microstructure is needed.

1.2 Creep Behavior of Superalloys

The creep behavior of single crystal superalloys is highly anisotropic. The inherent crystallography of single crystals leads to orientation dependent creep behavior. From a design point of view, it is imperative to use an orientation, which utilizes maximum strength of the superalloy. In fact it is known that the creep strength of a modern single crystal superalloy along the <001> orientation , which is also the preferred grain growth direction is favorable compared to the <011> or <111> orientations.

There have been numerous experimental investigations into the creep behavior and the related microstructural aspects of the <001> oriented single crystal nickel based superalloys. Apart from this, experiments have also focused on characterizing the behavior of single crystal turbine blades with centrifugal loading away from the exact <001> orientation. Such situations are common in actual practice where mis-alignment of up to 15° [33] could occur due to variety of reasons. A number of studies have been devoted to studying the creep performance of <001> oriented superalloy single crystals. At lower temperatures, particularly in the vicinity of 750 ^{o}C, a considerable amount of primary creep can occur (see [28] and [11]). At temperatures between 850 ^{o}C and 1000 ^{o}C, loading along <001> yields a creep strain rate which increases monotonically with creep strain (i.e., tertiary creep is dominant), there being no evidence of a steady state regime (See [5], [39] and [66]). At temperatures beyond 1000 ^{o}C, Reed *et al.* [64] reported that rafting of γ' phase occurs very rapidly and is complete in the very initial stages of creep deformation. After this stage, strain rate decreases with increasing strain for a considerable amount of time. Reed *et al.* [64] concluded that this strain hardening effect arises as a consequence of rafting of γ' phase. The strain rate in this temperature range keeps decreasing with increasing strain until a critical strain is reached. After the critical strain is reached, the creep

strain rate increase sharply with strain with failure occurring eventually. Moreover, this critical strain was found to be essentially constant in the temperature range of 1050-1200 ^{o}C. Reed *et al.* [64] observed that the rapid increase in the creep strain in the later stages of creep is associated with highly localized deformations in the vicinity of the fracture surface. Furthermore, this creep deformation is associated with creep cavitation occurring at, or in the vicinity of casting porosity and topologically closed packed (TCP) phases.

As pointed out earlier, the inherent crystallography of single crystals leads to orientation dependent creep behavior. The degree of anisotropy is strongly influenced by the temperature (around 750-850 ^{o}C) and it is also known that at higher temperatures, the orientation dependence of creep behavior is less strong. Several studies have been devoted to study the effect of orientation on creep behavior of single crystal superalloys and identify the slip systems responsible for the observed deformation behavior. Experiments carried out by Kear and Piearcey [23] on first generation single crystal nickel based superalloy MAR-M200 revealed that creep resistance close to the <001> and <111> orientations is substantially better than that close to the <011> orientation in the temperature range 760-871 ^{o}C. They also found that orientation has much less influence on creep life at 982 ^{o}C. It was also observed that at 760 ^{o}C, <001> orientation has the best creep life, however at temperatures 872 and 982 ^{o}C, <111> orientation displayed the best creep life. Significant amount of primary creep was observed close to the <001> orientation at 760 ^{o}C, however primary creep was absent for the <011> and <111> orientations. At temperatures beyond 760 ^{o}C, tertiary creep was dominant in all the orientations studied. Another experimental study on creep of MAR-M200 at 760 ^{o}C was performed by Leverant and Kear [27], wherein they studied the creep behavior of specimens oriented within 18° of <001> orientation. They observed primary, secondary and tertiary creep regimes for all the orientations and noted that the primary and steady state creep rates increase in the following order: <001>, <001>/<011> boundary, orientations between <001>/<011> and <001>/<111> boundaries, <001>/<111> boundary. A similar study performed by MacKay and Maier [29] on another first generation single crystal nickel based superalloy MAR-M247 at temperature 774 ^{o}C showed that crystals having orientations within 25° of the <001> orientation exhibited significantly longer creep lives when their orientations were closer to the <001>/<011> boundary of the stereographic triangle than to the <001>/<111> boundary. These observations were in accordance with the results for the creep of MAR-M200 ([37, 41]), the only difference being that MAR-M247 showed best creep life close to the <111> orientation whereas MAR-M200 showed best creep life close to the <001> orientation. Caron et al. [6] studied the effect of orientation on creep lives of first generation single crystal nickel based superalloy CMSX-2 at 760 ^{o}C and 750 MPa. Their experiments showed that the best creep life occurs close to the <001> orientation, however unlike the results for MAR-M200 and MAR-M247 [37, 41, 43], CMSX-2 exhibited very poor creep life close to the <111> orientation. Moreover, orientations away from the <001> orientation (say by 20°) did not cause significant reduction in creep life as was the case for MAR-M200 and MAR-M247 [37, 41, 43].

The effect of orientation on creep behavior of second generation single crystal nickel based superalloy CMSX-4 was studied by Matan et al. [32]. They studied the creep behavior for small misorientations away from the <001> orientation. Their investigation showed that at 750 ^{o}C, significant amount of primary creep takes place, the extent of which depends strongly upon small misorientations away from the <001>/<011> boundary of the stereographic triangle. At 950 ^{o}C, tertiary creep is dominant with very little primary creep. They also observed that orientation dependence is less strong at 950 ^{o}C. Recent creep tests carried out by Gunturi et al. [19] on CMSX-4 at 750 ^{o}C in crystallographic orientations distant from the <001> orientation showed that orientations distant from the <001>/<111> boundary had relatively lower creep lives while orientations closer to the <001>/<111> boundary had longer creep life.

1.3 Previous works on single crystals

Several models have been proposed to describe the response of single crystals. The notion of Bravais lattice has been associated with the structure of single crystals at the atomic level to model its behavior. The single crystals are not free of imperfections in that they have dislocations and inclusions which are responsible for the permanent inelastic deformation of single crystals. In polycrystals, the presence of grain boundaries complicate the material behavior signifcantly.

There are several studies on the kinematical aspects of crystals, under the assumption of uniformly distributed dislocations (see Bilby [3], Eshelby [13], Kondo [24], KrÄoner [25] and Nabarro [36]). A dynamical theory based for single crystals based on the notion of a Cosserat continuum via the introduction of directors was established by Naghdi and Srinivasa [41]. The theory based on the notion of directors has several inherent difficulties such as introduction of new balance laws containing terms which are not physically motivated. Moreover there are associated difficulties with regard to specifying boundary conditions for quantities such as directors. Naghdi and Srinivasa [40] have also introduced a measure of the influence of dislocations on the plastic deformation of single crystals through the curl of the plastic deformation gradient.

Early experiments on single crystals were carried out by Ewing and Resenhain [14], Taylor and Elam [71, 72, 73], Piercy et al. [44], and Kocks [45]. Piercy et al. [44] and Kocks [45] studied multiple slips in single crystals. Various mechanisms have been proposed to explain the response of single crystals and a discussion on these can be found in papers by Asaro [1], Havner [20], Taylor [70] and Van Buereu [98]. The most important issue to recognize, concerning the modeling of a single crystal is that it is not a simple material in the sense of Noll [43] (see also Truesdell and Noll [74]), that is the stress in the material can not be purely determined by the history of the deformation gradient. Several methods have been proposed to capture this non-simple behavior of the body (for example, the theory based on directors) but they are fraught with difficulties. One of the goals of the current work is to understand why the theory of simple materials fail for single crystals and to develop a rigorous approach to model such non-simple materials.

1.4 Current models for creep and shortcomings

There have been several attempts to model the creep behavior of single crystal superalloys. Phenomenological models have been developed both to describe the creep deformation of <001> oriented single crystals and to describe the orientation dependence of creep behavior. Dyson and Mclean [11] observed that the tertiary creep rate in most engineering materials including conventional nickel based superalloys increases monotonically with accumulated plastic strain. They concluded that strain softening is caused by active damage mechanisms (cavitation and development of cracks on the surface) and accumulation of dislocations. They excluded the possibility of γ' phase coarsening causing the strain softening as was thought earlier. They also presented an empirical model wherein the strain rate is determined by inelastic strain rather than time. Following their observations, several empirical models for

creep in superalloys have been proposed that take into account the kinetics of the dislocation motion [10]. The models developed in [11] and [10] are isotropic models and hence cannot capture orientation dependent creep behavior. An extension of the isotropic model to capture the anisotropic creep behavior was developed by Ghosh and Mclean [16] and Ghosh *et al.* [15]. Since the level of primary creep observed in most single crystal superalloys is small, they restricted their extension of anisotropy to the analysis of tertiary creep only and not to the primary creep. Their model accounted for tertiary creep based on the accumulation of mobile dislocations with plastic strain. Reed *et al.* [64] extended the model developed by Ghosh and co-workers to include the effect of rafting at high temperature.

Several other models for creep of superalloys have been proposed based on the framework of continuum damage mechanics and single crystal plasticity. Bertram and Olschewski [2] proposed an anisotropic constitutive model for describing creep behavior of single crystal superalloys. They constructed a three dimensional model by a projection technique which is essentially a generalization of the four-parameter Burgers model. Their model was restricted to the undamaged material behavior of the primary and secondary creep phase. Qi and Bertram [48] extended the model using the theory of continuum damage mechanics to incorporate the damage induced in the material through the introduction of a fourth order tensor that assesses damage.

Recently Maclachlan and Knowles [30] have proposed a model based on single crystal plasticity wherein they incorporate the damage induced due to creep through a fourth order damage operator. Most of the models for creep of single crystal superalloys fail to take into account the symmetry of single crystals and the fact that the symmetry does not change as the single crystal undergoes inelastic deformation. Apart from this, most of these models are empirical in nature and lacked a three dimensional framework. These models also lack thermodynamical underpinnings. Although models based on single crystal plasticity are three dimensional and they incorporate the symmetry of single crystals, such models require extensive details of slip systems which are operating. Also, the model requires information about self and latent hardening of slip systems that are active which lead to a overwhelming number of material parameters (The model developed by Maclachlan and Knowles [30] has 42 material parameters). The effect of high temperature rafting on creep was incorporated in models developed by Reed *et al.* [64] and Maclachlan and Knowles [30] who used a dislocation hardening mechanism first proposed by Gilman [17]. Apart from including the effect of rafting on creep in a macroscopic way, there have been several works devoted to describe the kinetics of the rafting behavior itself but most of them are limited to the elastic regime (see for example [63, 34, 35, 24, 25, 15, 54]). Such approaches are fraught with difficulties as the elastic regime is very difficult to detect in modern superalloys and rafting is always associated with significant amount of inelastic strain. Such a drawback was emphasized by the work of Carry and Strudel [10, 11], Ignat and co-workers [33, 7] and others where it was shown that interaction of dislocations created during creep deformation with $\gamma - \gamma'$ interface play an important role in morphological changes of precipitates. The models developed by Socrate and Parks [68] and Veron *et al.* [75] attempted to account for the inelastic strain, but their work was empirical in nature, lacked a 3D framework and was within the purview of small strain theory.

1.5 Goals of the current work

In this work, the aim is to develop a constitutive theory within the context of continuum mechanics, to predict the creep deformation of single crystal superalloys. The goal of such

continuum theories is to describe the macroscopic behavior of a material without explicitly going into the complex details at the microscopic level, while at the same time taking cognizance of the microstructure , albeit in a homogenized sense.

The constitutive model is within a thermodynamic setting and it exploits the fact that the configuration that the body would attain on the removal of external stimuli, referred to as "natural configuration", evolves, with the response of the body being non-dissipative (in more general situations non entropy producing) from these evolving "natural configurations". The evolution of these natural configurations is determined by the tendency of the body to undergo a process that maximizes the rate of dissipation.

As mentioned before, it is important to recognize that single crystals can not be modeled by theory of simple materials. The lattice structure and the material symmetry remains the same when a single crystal is subject to inelastic deformation. This experimental fact was recognized by the seminal work of Taylor and Elam [71] in as early as 1923. The current work aims to take cognizance of this essential empirical fact and develop a constitutive theory that complies with this observation. Another goal of the current work is to evaluate the theories based on single crystal plasticity which explicitly take into account elaborate details of the motion of dislocations on various slip systems and model the self and latent hardening of these systems during the inelastic deformation process. Such an elaborate detail is not needed to model the inelastic behavior of single crystals and a phenomenological continuum mechanics based model which take cognizance of the microstructure in a homogenized sense will suffice. As pointed out earlier, one of the shortcomings of incorporating elaborate details regarding motion of dislocations on slip systems and the hardening of slip systems is that one ends up with an overwhelming number of material parameters.

The constitutive model that has been developed is implemented in finite element software ABAQUS/STANDARD through a user subroutine (UMAT). The User Material has been developed and tested to ensure that the built in implicit creep integration routine based on a first order backward difference operator works well. The results obtained through the use of UMAT and those obtained using semi-inverse method work well. At this point the UMAT is ready to be used for solving real world problems.

2. DEVELOPEMT OF CONTINUUM MODEL FOR CREEP OF SUPERALLOYS

The model that has been developed is within the framework of multiple natural configurations developed by Rajagopal and coworkers. For materials undergoing large deformations, Eckart [12] seems to have been the first to recognize that many materials can possess multiple stress free states (natural configurations), that he called variable relaxed states, and studied them in some detail. However, he did not worry about symmetry considerations of the variable relaxed states or the role that the evolution of the symmetry plays in the constitutive relation for the material. Nor was Eckart interested in placing the evolution of material structure within a thermodynamic framework. A detailed discussion of the central role played by natural configurations in a variety of dissipative processes with associated symmetry changes and the change of the response characteristics of the body has been considered by Rajagopal [49, 50]. In fact the notion of "Natural configurations" is central to the development of constitutive theories in continuum mechanics. The crucial role it plays in describing the response of a broad range of material behaviors has not been recognized and delineated in detail until the recent work of Rajagopal [49,

50]. Invoking the notion of "natural configurations" has led to the development of constitutive theories which has filled the lacunae that existed in incorporating the microstructural details from a continuum perspective. It has led to development of constitutive theories with rigorous thermodynamic underpinnings without resorting to any ad hoc means such as invoking "internal variables" into the theory. The phenomenal success of such a framework in describing the response of a disparate class of materials can be seen in a series of papers by Rajagopal and coworkers: the response of multi-network polymers [77, 61], twinning [52, 53], traditional plastic response [54, 55], solid to solid phase transitions [52, 53], shape memory alloys [56], viscoelastic response [57], anisotropic response of liquids [58], crystallization of polymers [63], superplastic response [51], response of asphalt mixtures [35], growth and adaptation of biological materials [62] and response of superalloys [47]. The classical theories of elasticity and linearly viscous fluid arise naturally as sub-cases. The framework of multiple natural configurations exploits the fact that the configuration that the body would attain on the removal of external stimuli, referred to as "natural configuration", evolves, with the response of the body being non-dissipative (in more general situations non entropy producing) from these evolving natural configurations. The evolution of these natural configurations is determined by the tendency of the body to undergo a process that maximizes the rate of dissipation. Different natural configurations are accessed during different processes. It is suffice to say that the notion of natural configuration is a primitive in our framework and it can be thought of as one of the state variables in the constitutive theory.

2.1 Development of constitutive model

Let us now start with the reduced energy dissipation equation (see Green and Naghdi [18]):

$$\mathbf{T} \cdot \mathbf{L} - \rho\dot{\psi} - \rho\eta\dot{\theta} - \frac{\mathbf{q} \cdot \mathrm{grad}(\theta)}{\theta} = \rho\theta\xi := \zeta \geq 0 \ ,$$

where where T is the Cauchy stress, ρ is the density, ψ is the Helmholtz potential, η is the specific entropy, θ is the absolute temperature, q is the heat flux vector, n is the rate of entropy production and f is the rate of dissipation.

In what follows, the effect of temperature is ignored and an isothermal model is developed. The motivation to develop an isothermal model stems from the fact that all the creep experiments are done at a constant temperature. The material parameters that will appear in the constitutive model will be different for different temperatures.

Splitting the entropy production part as that due to thermal effects and a part due to mechanical dissipation lead us to,

$$\mathbf{T} \cdot \mathbf{L} - \rho\dot{\psi} = \zeta_{mech} \geq 0 \ .$$

This equation is the starting point for the development of an isothermal constitutive model.

The form for the stored energy of the crystalline materials is assumed to be

$$\psi = \psi(\mathbf{F}_{\kappa_{p(t)}}, \mathbf{G}) \ .$$

It is assumed that the Helmholtz potential can be decomposed in the following way:

$$\psi = \hat{\psi} + \tilde{\psi} \ ,$$

where

$$\hat{\psi} = \hat{\psi}_{\kappa_{p(t)}}(\mathbf{F}_{\kappa_{p(t)}}) \ ,$$

is related to the elastic stored energy, and

$$\tilde{\psi} = \mathcal{F}_{\tau=0}^{\infty}[\mathbf{G}(t - \tau)] \ ,$$

is related to the inelastic stored energy. A standard rearrangement will yield

$$\left[\mathbf{T} - \rho\frac{\partial\hat{\psi}}{\partial\mathbf{F}_{\kappa_{p(t)}}}\mathbf{F}^{T}_{\kappa_{p(t)}}\right] \cdot \mathbf{L} + \rho\mathbf{F}^{T}_{\kappa_{p(t)}}\frac{\partial\hat{\psi}}{\partial\mathbf{F}_{\kappa_{p(t)}}} \cdot \mathbf{L}_{p} - \rho\frac{d\tilde{\psi}}{dt} = \zeta_{mech} \geq 0 \ .$$

It is now assumed that the Cauchy stress is of the form

$$\mathbf{T} = \rho\frac{\partial\hat{\psi}}{\partial\mathbf{F}_{\kappa_{p(t)}}}\mathbf{F}^{T}_{\kappa_{p(t)}} = \rho\mathbf{F}_{\kappa_{p(t)}}\frac{\partial\hat{\psi}}{\partial\mathbf{E}_{\kappa_{p(t)}}}\mathbf{F}^{T}_{\kappa_{p(t)}} \ .$$

On using the form for the Cauchy stress, the reduced dissipation equation can be decomposed to

$$\mathbf{A} \cdot \mathbf{D}_{p} + \tau \cdot \mathbf{W}_{p} - \rho\frac{d\tilde{\psi}}{dt} = \zeta_{mech} \ ,$$

where

$$\mathbf{A} = (\mathbf{F}^{T}_{\kappa_{p(t)}}\mathbf{T}\mathbf{F}^{-T}_{\kappa_{p(t)}})_{sym} = \frac{1}{2}\mathbf{R}^{T}_{\kappa_{p(t)}}(\mathbf{V}_{\kappa_{p(t)}}\mathbf{T}\mathbf{V}^{-1}_{\kappa_{p(t)}} + \mathbf{V}^{-1}_{\kappa_{p(t)}}\mathbf{T}\mathbf{V}_{\kappa_{p(t)}})\mathbf{R}_{\kappa_{p(t)}} \ ,$$

$$\tau = (\mathbf{F}^{T}_{\kappa_{p(t)}}\mathbf{T}\mathbf{F}^{-T}_{\kappa_{p(t)}})_{skew} = \frac{1}{2}\mathbf{R}^{T}_{\kappa_{p(t)}}(\mathbf{V}_{\kappa_{p(t)}}\mathbf{T}\mathbf{V}^{-1}_{\kappa_{p(t)}} - \mathbf{V}^{-1}_{\kappa_{p(t)}}\mathbf{T}\mathbf{V}_{\kappa_{p(t)}})\mathbf{R}_{\kappa_{p(t)}} \ .$$

For a material that is elastically isotropic, $\mathbf{T}$ will be an isotropic function of $\mathbf{V}_{\kappa_{p(t)}}$ so that $\tau = 0$.

The rate of dissipation due to creep is assumed to be of the form

$$\zeta_{mech} = \zeta_1(\theta, \mathbf{D}_p) + \zeta_2(\theta, \mathbf{W}_p) \;,$$

i.e., the rate of dissipation depends both upon the rate at which the material stretches as well as the rate at which the orientation changes. For a specimen loaded in any arbitrary orientation, the crystal lattice rotates. However, for uniaxial creep loading along orientations <001>, <111> and <011>, there is no associated rotation of the crystal lattice.

Reducing the decomposed reduced dissipation equation further yields

$$\mathbf{A} \cdot \mathbf{D}_p - \rho \frac{d\tilde{\psi}}{dt} = \zeta_1(\theta, \mathbf{D}_p) \;, \quad \tau \cdot \mathbf{W}_p = \zeta_2(\theta, \mathbf{W}_p) \;.$$

2.2 Specific constitutive relations

2.2.1 The Helmholtz potential

The specific form for the elastic stored energy consistent with a crystal having cubic symmetry is

$$\hat{\psi} = \frac{1}{2\rho} \Big[c_{12}(\mathrm{tr}\, \mathbf{E}_{\kappa_{p(t)}})^2 + 2c_{44}(\mathrm{tr}\, \mathbf{E}^2_{\kappa_{p(t)}}) + (c_{11} - c_{12} - 2c_{44})\big((\mathbf{a} \cdot \mathbf{E}_{\kappa_{p(t)}}\mathbf{a})^2 +$$
$$(\mathbf{b} \cdot \mathbf{E}_{\kappa_{p(t)}}\mathbf{b})^2 + (\mathbf{c} \cdot \mathbf{E}_{\kappa_{p(t)}}\mathbf{c})^2\big) \Big] \;,$$

where $\mathbf{a}$, $\mathbf{b}$ and $\mathbf{c}$ are orthogonal unit vectors along the principal cubic axes and c_{11}, c_{12} and c_{44} are three independent parameters characterizing the elastic response.

2.2.2 Inelastic part of the stored energy

The form for the inelastic stored energy captures the part of mechanical work that is trapped in the dislocation networks. Models due to Lee [26], Brown et al. [4] and Mason et al. [31] account for this kind of energy storage mechanism in the body by multiplying the "plastic work" by an ad hoc factor whose value is approximately 0.8. The current work utilizes a rigorous form for such an energy storage mechanism without resorting to any ad hoc means. The energy that is stored in dislocation networks is of tremendous importance during the inelastic deformation of single crystal superalloys as such superalloys are multi phase materials with their microstructure engineered in such a way to ensure solid solution hardening and precipitation hardening.

We will assume the following form for the inelastic part of the free energy $\tilde{\psi}$ developed by Mollica et al., [34] and subsequently used by Prasad et al., [47]:

$$\tilde{\psi} = \psi_1 a(s) + \psi_2 \int_0^s e^{\eta(x-s)} \big(\mathbf{E}_p(s) - \mathbf{E}_p(x)\big) \cdot \mathbf{N}(x) dx \;,$$

where the scalar variable $s = s(t)$ is referred to as "inelastic strain pathlength" and is defined as

$$\dot{s} = (\mathbf{D}_p \cdot \mathbf{D}_p)^{\frac{1}{2}} \ ,$$

ψ_1, ψ_2 and η are material constants and

$$\mathbf{E}_p = \int_0^t \mathbf{D}_p(\tau)d\tau \ ,$$

$$\mathbf{N} = \frac{\mathbf{D}_p}{(\mathbf{D}_p \cdot \mathbf{D}_p)^{\frac{1}{2}}} \ .$$

$\mathbf{E}_p$ is a measure of accumulated inelastic strain with reference to reference configuration and it can be described as a measure of the total amount of slip that has taken place on slip systems which are active [42].

Also, $a(s)$ is the density of the dislocation network (defined as the total length of dislocation lines per unit volume [65]) and assumes the following form:

$$a(s) = a_o(1 + \beta_2(1 - e^{-\alpha_1 s})) \ .$$

The motivation to choose such a form stems from the experimental observation that the dislocation density increases with monotonic inelastic deformation and reaches a saturation value after a while.

The time rate of change of inelastic part of stored energy is given by

$$\rho \frac{d\tilde{\psi}}{dt} = \rho \left[\psi_1 \left(a' + \eta a \right) - \eta \tilde{\psi} \right] (\mathbf{D}_p \cdot \mathbf{D}_p)^{\frac{1}{2}} + \left(\rho \psi_2 \int_0^s e^{\eta(x-s)} \mathbf{N}(x)dx \right) \cdot \mathbf{D}_p \ ,$$

$$:= h(s)(\mathbf{D}_p \cdot \mathbf{D}_p)^{\frac{1}{2}} + \alpha \cdot \mathbf{D}_p \ ,$$

where $(.)'$ denotes the total derivative with respect to s.

The tensor

$$\alpha = \rho \psi_2 \int_0^s e^{\eta(x-s)} \mathbf{N}(x)dx \ ,$$

is the backstress tensor. On taking the time derivative of the expression for backstress tensor, it can be seen that the backstress, would satisfy the following evolution equation:

$$\dot{\alpha} = \rho\psi_2 \mathbf{D}_p - \eta(\mathbf{D}_p \cdot \mathbf{D}_p)^{\frac{1}{2}}\alpha \ ,$$

which is a generalized version of the non-linear kinematic hardening rule [7]. Although no experimental data concerning the inelastic stored energy is available, to our knowledge, for single crystal superalloys, there are experimental data for polycrystalline metals [3, 76]. Apart from the experiments, several attempts have been made to model the inelastic stored energy (see for example, papers by Chaboche [13, 14] and Kamlah and Haupt [22]). The inelastic stored energy might not be significant at high temperatures at which creep occurs as only a small fraction of energy is stored (dissipation mechanisms being dominant).

2.2.3. Rate of dissipation

Following form for the rate of dissipation is assumed:

$$\zeta_1 = \mathbf{D}_p \cdot \mathbf{K}\mathbf{D}_p \ , \quad \zeta_2 = \eta_2 \mathbf{W}_p \cdot \mathbf{W}_p \ ,$$

where $\mathbf{K}$ is a fourth order tensor reflecting cubic symmetry that is a function of the temperature, the inelastic history of the material and the driving force:

$$\mathbf{K} = k_{12}\mathbf{I} \otimes \mathbf{I} + 2k_{44}\mathbf{I}_4 + (k_{11} - k_{12} - 2k_{44})\mathcal{N} \ ,$$

where $\mathbf{I}_4$ is the fourth order identity tensor, and the fourth order tensor $\mathcal{N}$ has the form

$$\mathcal{N}_{ijkl} = a_i a_j a_k a_l + b_i b_j b_k b_l + c_i c_j c_k c_l \ .$$

a_i, b_i and c_i are the components of the orthogonal unit vectors $\mathbf{a}$, $\mathbf{b}$ and $\mathbf{c}$. The evolution equation for the natural configuration is determined by the tendency of the body to undergo a process that maximizes the rate of dissipation. The idea of maximization of rate of dissipation is not a fundamental principle of thermodynamics. However it is also not ad hoc either. It is a generalization of a notion due to Gibbs that an isolated system tends to a state of maximal entropy. A further assumption is made that the way, the body gets to the state of maximal entropy is by producing entropy at the maximal possible rate (see Rajagopal and Srinivasa [59, 60]).

Maximizing the rate of dissipation subject to the constraint $tr(\mathbf{D}_p) = 0$ (inelastic deformation being isochoric) gives the following equations for $\mathbf{D}_p$ and $\mathbf{W}_p$:

$$\mathbf{A} = p\mathbf{I} + \mathbf{A}^* \ ,$$

$$\mathbf{A}^* = \alpha + \mathbf{K}\mathbf{D}_p + h(s)\frac{\mathbf{D}_p}{(\mathbf{D}_p \cdot \mathbf{D}_p)^{\frac{1}{2}}} \ ,$$

$$p = \frac{1}{3}tr(\mathbf{A} - \mathbf{A}^*) \ ,$$

and

$$W_p = \frac{1}{\eta_2}\tau .$$

The rate of dissipation functions are required to be non-negative. Our constitutive assumption for the rate of dissipation ensures that it is non-negative. The rate of dissipation is dependent on the fourth order tensor K which is anisotropic. It is assumed that two mechanisms contribute to the rate of dissipation in the following way:

The first mechanism is related to the dissipation caused by mobile dislocations. There is a rapid multiplication of dislocations in the γ matrix at the beginning of creep. It is observed that the γ' phase is "hard" for significant amount of creep strains and hence no dislocation activity is associated with it. As the deformation increases, these dislocations start moving in the γ matrix. Further deformation results in these dislocations being stuck and bowed. This causes "hardening" of the material. In order to describe the loss of mobility of the dislocations with accumulating "creep strain", it is assumed that the mean velocity of the dislocations remains constant at constant stress while the density of dislocations, which are mobile decay exponentially. That is, only a fraction of the total remains mobile. Let f be this fraction. In accordance with the work of Gilman [17], following form for the mobile fraction is assumed:

$$f = e^{\alpha_2 s},$$

where α_2 is the attrition coefficient.

The density of mobile dislocations, $a_m(s)$ is then given by

$$a_m(s) = a(s)f = a_o(1 + \beta_2(1 - e^{-\alpha_1 s}))e^{-\alpha_2 s}.$$

The first mechanism of dissipation is assumed to be proportional to the inelastic strain pathlength, $s(t)$ in the following way:

$$\zeta_1 \propto a_m(s).$$

Apart from this, the dissipation mechanism, in general, also depends upon the driving force, as most dislocation interactions become less inhibitory with increasing driving force.

The second mechanism associated with dissipation is related to the damage accumulation by creep cavitation. With the creep strain accumulating, the material starts getting "damaged' by means of highly localized deformation in the vicinity of crack surfaces. As reported in numerous experiments, this creep elongation at the later stage of deformation is associated with creep cavitation occurring at, or in the vicinity of casting porosity and topologically closed-packed phases. Hence this stage is marked by a rapid increase in the strain ("softening"). Moreover, experiments clearly indicate that the effect of highly localized damage due to creep cavitation becomes dominant only after a certain critical strain is reached. The second mechanism of dissipation is assumed to be proportional to the inelastic strain pathlength, $s(t)$ in the following way:

$\zeta_1 \propto e^{\alpha_3 s}.$

Moreover, it is also assumed that this second mechanism of dissipation remains active throughout the creep process but becomes dominant only in the later stages of creep. This second mechanism, in general, is also dependent on the driving force.

The coefficients associated with the tensor **K** have the following form:

$$k_{11} - k_{12} = \frac{1}{\beta_1 e^{\kappa_1 tr(\mathbf{A})} a(s) e^{-\alpha_2 s} + \beta_3 e^{\kappa_2 tr(\mathbf{A})} e^{\alpha_3 s}},$$

$$k_{44} = \frac{0.5}{\Lambda_1 e^{\Gamma_1 tr(\mathbf{A})} a(s) e^{-\Omega_2 s} + \Lambda_3 e^{\Gamma_2 tr(\mathbf{A})} e^{\Omega_3 s}}.$$

It should be noted that k_{11}, k_{12} and k_{44} have the same form. The material parameters ψ_1, ψ_2 and η and which are associated with the inelastic stored energy do not change with the orientation of the crystal. The form for the rate of dissipation function is motivated based on creep deformation when the specimen is loaded along the <001> and the <111> directions. The coefficients k_{11} - k_{12} and k_{44} reflect the dissipation which takes place when the specimen is loaded in the <111> and the <001> direction, respectively. Such a description is a simplistic one and we will see that it captures the creep deformation of single crystal superalloys reasonably well. The dependence of rate of dissipation on dislocation motion is much more intricate when the specimen is loaded along arbitrary directions.

2.2.4. Instantaneous rate of energy storage, *R*

One of the important quantities in any inelastic process is the ratio of rate of energy stored to the rate of work done by the externally applied tractions. The rate at which work is done during the inelastic process by the applied tractions per unit mass is given by

$$w_i(t) = \frac{\mathbf{T} \cdot \mathbf{L}}{\rho}.$$

The rate of dissipation per unit mass is given by

$$w_d(t) = \frac{\zeta_{mech}}{\rho} = \frac{1}{\rho}(\mathbf{D}_p \cdot \mathbf{K}\mathbf{D}_p + \eta_2 \mathbf{W}_p \cdot \mathbf{W}_p).$$

The instantaneous rate of energy storage, *R* is then given by

$$R = \frac{w_s(t)}{w_i(t)} = 1 - \frac{w_d(t)}{w_i(t)},$$

where the equation of balance of energy is utilized in the form of reduced energy dissipation equation. Although no experiments have been conducted, to our knowledge, on single crystal superalloys to measure such a quantity, there are some experimental results for polycrystalline metals (see Williams [76]) which can provide some guidance in our choice for the same for single crystal superalloys.

3. RESULTS AND DISCUSSIONS

CREEP OF SUPERALLOYS LOADED ALONG THE <001>, <111> AND <011> ORIENTATIONS

Creep deformation of single crystal superalloys under loading in any arbitrary direction is fully three dimensional. However, uniaxial creep loading along the orientations <001>, <111> and <011> gives rise to a simple deformation field and there is no associated rotation of the crystal lattice.

We will assume the following form for the deformation in rectangular coordinates:

$$x(t) = \phi_1(t)X \; , \quad y(t) = \phi_2(t)Y \; , z(t) = \phi_3(t)Z \; ,$$

where (X, Y, Z) is a material point in the configuration $\cdot R$ and $(x; y; z)$, the corresponding material point in the configuration $\cdot t$.

The deformation gradient associated with the above motion is given by

$$\mathbf{F} = \mathrm{diag}(\; \phi_1(t), \; \phi_2(t), \; \phi_3(t)) \; .$$

The symmetric and skew part of $\mathbf{L}_p$ are given by

$$\mathbf{D}_p = \mathrm{diag}\left(\frac{\dot{\phi}_1(t)}{\phi_1(t)}, \; \frac{\dot{\phi}_2(t)}{\phi_2(t)}, \; \frac{\dot{\phi}_3(t)}{\phi_3(t)} \right) \; , \quad \mathbf{W}_p = 0 \; ,$$

which leads us to the governing equations for the motion:

$$\left(\frac{h}{\dot{s}} + 2k_{44} \right) \frac{\dot{\phi}_i(t)}{\phi_i(t)} + (\mathcal{N}\mathbf{D}_p)_i = (\mathbf{A})_i - p - (\alpha)_i \; ,$$

$$(\dot{\alpha})_i = \rho\psi_2 \frac{\dot{\phi}_i(t)}{\phi_i(t)} - \eta\dot{s}(\alpha)_i \; , \quad i = 1 - 3 \; (\text{no sum on } i) \; ,$$

$$\dot{\tilde{\psi}} = \frac{1}{\rho}\left(h\dot{s} + (\alpha)_1 \frac{\dot{\phi}_1(t)}{\phi_1(t)} + (\alpha)_2 \frac{\dot{\phi}_2(t)}{\phi_2(t)} + (\alpha)_3 \frac{\dot{\phi}_3(t)}{\phi_3(t)} \right) \; ,$$

where $()_i$ denotes the i-th diagonal element of the respective second order tensors. The above equations form the set of governing non-linear ordinary differential equations.

3.1 Results for loading along the <001> orientation

The creep strain was obtained by integrating the above equations over time. These equations are solved using a solver (ODE15S) for initial value problems in MATLAB. The results were obtained for a range of temperatures, which are pertinent to the problem under consideration. The material parameters, in general, are functions of temperature. Simulation was carried out at three di®erent temperatures at various stress values and the results are compared with the experimental results for CMSX-4 ([69] and [21]).

The variation of creep strain, instantaneous rate of energy storage and inelastic stored energy with time are presented for different temperatures at various stresses. The variation of creep strain with time for θ = 750, 982 and 1000 ^{o}C are shown in Figs. 5, 6 and 7. It can be seen that the predictions of the model agree well with the experimental data for the different temperatures considered here. Figs. 8, 9 and 10 depict the variation of the inelastic stored energy with respect to the inelastic strain pathlength. Also, Figs. 11, 12 and 13 represent the variation of third component of backstress tensor with inelastic strain pathlength. Variation of the instantaneous rate of energy storage with inelastic strain pathlength is also studied. It can be seen from Figs. 14, 15 and 16 that the material stores energy in the initial stages of deformation but as the deformation proceeds most of the energy is dissipated.

Moreover, it can be observed that the fraction of energy stored decreases at higher temperatures. That is, at higher temperatures most of the work done by the applied tractions is dissipated. This is to be expected as the dislocation motion which is primarily the source of dissipation becomes less and less inhibitory as the temperature increases. The inelastic stored energy increases with inelastic deformation but its value seems to be attaining a saturation value. The driving force doesn't seem to have significant effect on the variation of inelastic stored energy as the curves for the different stresses lie almost on top of each other. The driving force however, has significant effect on the rate of dissipation as dissipation mechanisms themselves are strongly dependent on the driving force.

3.2 Results for loading along the <001>, <111> and <011> orientations

The set of ordinary differential equations are solved using an initial value problem solver in MATLAB (ODE15s). The material parameters associated with coefficient $k44$ are fixed by matching the results with experiments for loading along the <001> orientation. Similarly, the parameters in the expression for k_{11}-k_{12} are fixed by matching the results with experiments for loading along the <111> orientation. Hence, the orientations <001> and <111> are complete for determining the material constants for the current set of orientations studied. Once the complete set of materials parameters are obtained from the <001> and <111> data set, these are used to simulate the uniaxial creep along the <011> orientation. The results for single crystal nickel based superalloy CMSX-4 for loading along the <001>, <111> and <011> orientations for various values of stresses at 800 ^{o}C and 950 ^{o}C are obtained and compared with the available experimental results ([67, 45]). It is worth emphasizing that the material parameters are fixed with respect to one experiment and they are then used to predict the results for a different experiment.

The variation of the creep strain with time is shown in Figs. 17-22. It can be seen that the predictions of the model agree well with the experimental data for the temperatures considered here. The experimental data for loading along <011> orientation acts as a test case for measuring the efficacy of our model. Although no such data is available for 800 ^{o}C, we find that the prediction of the model are satisfactory for loading along the <011> orientation at 950 ^{o}C (see Fig. 22). Figs. 23 and 24 depict the variation of the inelastic stored energy with inelastic strain pathlength. The inelastic energy increases with inelastic deformation and eventually attains a saturation value. Neither the driving force nor the orientation seems to have any effect on the variation of inelastic stored energy as the curves for different stresses and loading orientations lie almost on top of each other. Figs. 25 and 26 show the variation of the third component of backstress tensor with inelastic strain pathlength. For certain orientations, the driving force seems to have little or no effect on the backstress, though for comparable stress values, the value of the backstress is somewhat lower for the <011> orientation than for the <001> and the <111> orientations. Variation of the instantaneous rate of energy storage with inelastic strain pathlength is depicted in Figs. 27 and 28. It can be seen that the material stores energy in the initial stages of deformation but as the deformation proceeds most of the energy is dissipated. For certain orientations, the fraction of energy stored decreases as the stress increases. This is expected as the dislocation motion which is primarily the source of dissipation becomes less and less inhibitory as the stress increases.

IMPLEMENTATION IN FINITE ELEMENT SOFTWARE ABAQUS

The constitutive model that has been developed is implemented in finite element software ABAQUS/STANDARD through a user subroutine (UMAT).

For the large deformation analysis based on continuum formulation, ABAQUS sends, for each integration point, the values of total deformation gradient, F at the current time t, the deformation gradient from the current natural configuration, Fe at current time t, current value of the Cauchy stress, T and the state variables such as s and G at the current time step. It also sends an estimate of the total deformation gradient at the next time step $(t + \Delta t)$. The UMAT supplies the values of the state variables such as s, $\mathbf{F}_e$ and $\mathbf{G}$ and Cauchy stress at time step $t + \Delta t$ and return it back to the ABAQUS. This process continues until the a converged solution is obtained at time step $t + \Delta t$. In estimating the value of total deformation gradient at time $t + \Delta t$, ABAQUS uses the value of the jacobian, J which is specified in the UMAT. An exact definition of the consistent jacobian is necessary to ensure quadratic convergence however the jacobian is often approximated in favor of a simpler algorithm and computational speed. This may result in the loss of quadratic convergence. In the current work, we have also used an approximate jacobian which is the same as the elasticity matrix for a face centered cubic crystal.

Let us now develop the numerical scheme based on implicit first order backward difference formula (backward Euler method). For the sake of completeness let us now list the equations describing the constitutive model. For the case when the rate of dissipation is assumed to be isotropic, the equations describing the constitutive model reduces to

$$\mathbf{D}_p = \frac{\dot{s}}{h + 2k_{44}\dot{s}} \left(\mathbf{A} - \frac{1}{3}tr(\mathbf{A})\mathbf{I} - \alpha \right) ,$$

$$:= \frac{\dot{s}}{h + 2k_{44}\dot{s}} \bar{\mathbf{A}} .$$

Using the definition for inelastic strain pathlength, we can get an explicit expression:

$$\dot{s} = \frac{1}{2k_{44}} \left(\sqrt{\bar{\mathbf{A}} \cdot \bar{\mathbf{A}}} - h \right) .$$

which leads to

$$\dot{\psi} = \frac{1}{\rho} \left(h + \frac{\alpha \cdot \bar{\mathbf{A}}}{\sqrt{\bar{\mathbf{A}} \cdot \bar{\mathbf{A}}}} \right) \dot{s} .$$

$$\dot{\alpha} = \left(\rho\psi_2 \frac{\bar{\mathbf{A}}}{\sqrt{\bar{\mathbf{A}} \cdot \bar{\mathbf{A}}}} - \eta\alpha \right) \dot{s} ,$$

Discreatizing the above equations using first order backward difference, we arrive at the following algebraic non-linear equations.

$$f_1 := {}^{t+\Delta t}s - {}^{t}s - \frac{\Delta t}{2^{t+\Delta t}k_{44}}\left(\sqrt{{}^{t+\Delta t}\bar{\mathbf{A}} \cdot {}^{t+\Delta t}\bar{\mathbf{A}}} - {}^{t+\Delta t}h\right) = 0 ,$$

$$f_2 := {}^{t+\Delta t}\tilde{\psi} - {}^{t}\tilde{\psi} - \frac{\left({}^{t+\Delta t}s - {}^{t}s\right)}{\rho}\left({}^{t+\Delta t}h - \frac{\Delta t {}^{t+\Delta t}\alpha \cdot {}^{t+\Delta t}\bar{\mathbf{A}}}{{}^{t+\Delta t}h\Delta t + 2^{t+\Delta t}k_{44}\left({}^{t+\Delta t}s - {}^{t}s\right)}\right) = 0 ,$$

$$f_3 := {}^{t+\Delta t}\alpha - {}^{t}\alpha + \eta\, {}^{t+\Delta t}\alpha\left({}^{t+\Delta t}s - {}^{t}s\right) - \frac{\rho\psi_2\Delta t\, {}^{t+\Delta t}\bar{\mathbf{A}}\left({}^{t+\Delta t}s - {}^{t}s\right)}{{}^{t+\Delta t}h\Delta t + 2^{t+\Delta t}k_{44}\left({}^{t+\Delta t}s - {}^{t}s\right)} = 0 .$$

This set of equations is solved using Newton-Raphson method.

CONCLUSIONS:

The numerical scheme developed in the previous section is implemented in UMAT to study the creep behavior of single crystal superalloys loaded along the <001> orientation. The UMAT is validated by using it to obtain the results already obtained in previous sections using the semi-inverse approach. The results obtained through the UMAT is compared with the results obtained using the semi-inverse approach and the experimental results. Figs. 29, 30 and 31 show a comparison of strain versus time curves for loading along <001> orientation at temperatures $\theta = 750$, 982 and 1000 ^{o}C obtained using the UMAT and the semi-inverse method and experimental results. Figs. 32, 33 and 34 show a comparison for the inelastic stored energy at temperatures $\theta = 750$, 982 and 1000 ^{o}C. A similar comparison is shown for third component of the backstress tensor in Figs. 35, 36 and 37. Figs. 38, 39 and 40 show the same comparison for instantaneous rate of energy storage.

GRAPHICAL MATERIALS LIST

Figure 1: Natural configurations associated with the body

Figure 2: Noll's rule for simple materials

Figure 3: Shearing of lattice of a single crystal

Figure 4: Creep of a specimen under constant load

Figure 5: Strain vs. time for CMSX-4 for loading along the <001> orientation, θ = 750 ^{o}C: Comparison of the predictions of the model with experimental results of Svoboda and Lucas [69] and Henderson and Lindblom [21].

Figure 6: Strain vs. time for CMSX-4 for loading along the <001> orientation, θ = 982 ^{o}C: Comparison of the predictions of the model with experimental results of Svoboda and Lucas [69] and Henderson and Lindblom [21].

Figure 7: Strain vs. time for CMSX-4 for loading along the <001> orientation, θ = 1000 ^{o}C: Comparison of the predictions of the model with experimental results of Svoboda and Lucas [69] and Henderson and Lindblom [21].

Figure 8: Inelastic stored energy vs. inelastic strain pathlength for CMSX-4 for loading along the <001> orientation, θ = 750 ^{o}C: Predictions of the model.

Figure 9: Inelastic stored energy vs. inelastic strain pathlength for CMSX-4 for loading along the <001> orientation, θ = 982 ^{o}C: Predictions of the model.

Figure 10: Inelastic stored energy vs. inelastic strain pathlength for CMSX-4 for loading along the <001> orientation, θ = 1000 ^{o}C: Predictions of the model.

Figure 11: Third component of backstress vs. inelastic strain pathlength for CMSX-4 for loading along the <001> orientation, θ = 750 ^{o}C: Predictions of the model.

Figure 12: Third component of backstress vs. inelastic strain pathlength for CMSX-4 for loading along the <001> orientation, θ = 750 ^{o}C: Predictions of the model.

Figure 13: Third component of backstress vs. inelastic strain pathlength for CMSX-4 for loading along the <001> orientation, θ = 1000 ^{o}C: Predictions of the model.

Figure 14: Instantaneous rate of energy storage vs. inelastic strain pathlength for CMSX-4 for loading along the <001> orientation, θ = 750 ^{o}C: Predictions of the model.

Figure 15: Instantaneous rate of energy storage vs. inelastic strain pathlength for CMSX-4 for loading along the <001> orientation, μ = 982 oC: Predictions of the model.

Figure 16: Instantaneous rate of energy storage vs. inelastic strain pathlength for CMSX-4 for loading along the <001> orientation, θ = 1000 ^{o}C: Predictions of the model.

Figure 17: Strain vs. time for CMSX-4 for loading along the <001> orientation, θ = 800 ^{o}C: Comparison of the predictions of the model with experimental results of Schubert et al., [67].

Figure 18: Strain vs. time for CMSX-4 for loading along the <111> orientation, θ = 800 ^{o}C: Comparison of the predictions of the model with experimental results of Schubert et al., [67].

Figure 19: Strain vs. time for CMSX-4 for loading along the <011> orientation, θ = 800 ^{o}C: Predictions of the model.

Figure 20: Strain vs. time for CMSX-4 for loading along the <001> orientation, θ = 950 ^{o}C: Comparison of the predictions of the model with experimental results of MacLachlan et al., [30].

Figure 21: Strain vs. time for CMSX-4 for loading along the <111> orientation, θ = 950 ^{o}C: Comparison of the predictions of the model with experimental results of MacLachlan et al., [30].

Figure 22: Strain vs. time for CMSX-4 for loading along the <011> orientation, θ = 950 ^{o}C: Comparison of the predictions of the model with experimental results of MacLachlan et al., [30].

Figure 23: Inelastic stored energy vs. inelastic strain pathlength for CMSX-4 , θ = 800 ^{o}C: Predictions of the model.

Figure 24: Inelastic stored energy vs. inelastic strain pathlength for CMSX-4 , θ = 950 ^{o}C: Predictions of the model.

Figure 25: Third component of backstress vs. inelastic strain pathlength for CMSX-4 , θ = 800 ^{o}C: Predictions of the model.

Figure 26: Third component of backstress vs. inelastic strain pathlength for CMSX-4 , θ = 950 ^{o}C: Predictions of the model.

Figure 27: Instantaneous rate of energy storage vs. inelastic strain pathlength for CMSX-4 , θ = 800 ^{o}C: Predictions of the model.

Figure 28: Instantaneous rate of energy storage vs. inelastic strain pathlength for CMSX-4 , θ = 950 ^{o}C: Predictions of the model.

Figure 29: Strain vs. time for CMSX-4 for loading along the <001> orientation, θ = 750 ^{o}C: Comparison of the results obtained from User Material in ABAQUS with results obtained in MATLAB and experimental results of Svoboda and Lucas [69] and Henderson and Lindblom [21].

Figure 30: Strain vs. time for CMSX-4 for loading along the <001> orientation, θ = 982 ^{o}C: Comparison of the results obtained from User Material in ABAQUS with results obtained in MATLAB and experimental results of Svoboda and Lucas [69] and Henderson and Lindblom [21]

Figure 31: Strain vs. time for CMSX-4 for loading along the <001> orientation, θ = 1000 ^{o}C: Comparison of the results obtained from User Material in ABAQUS with results obtained in MATLAB and experimental results of Svoboda and Lucas [69] and Henderson and Lindblom [21].

Figure 32: Inelastic stored energy vs. inelastic strain pathlength for CMSX-4 for loading along the <001> orientation, θ = 750 ^{o}C: Comparison of the results obtained from User Material in ABAQUS with results obtained in MATLAB.

Figure 33: Inelastic stored energy vs. inelastic strain pathlength for CMSX-4 for loading along the <001> orientation, θ = 982 ^{o}C: Comparison of the results obtained from User Material in ABAQUS with results obtained in MATLAB.

Figure 34: Inelastic stored energy vs. inelastic strain pathlength for CMSX-4 for loading along the <001> orientation, θ = 1000 ^{o}C: Comparison of the results obtained from User Material in ABAQUS with results obtained in MATLAB.

Figure 35: Third component of backstress vs. inelastic strain pathlength for CMSX-4, θ = 750 ^{o}C: Comparison of the results obtained from User Material in ABAQUS with results obtained in MATLAB.

Figure 36: Third component of backstress vs. inelastic strain pathlength for CMSX-4, θ = 982 ^{o}C: Comparison of the results obtained from User Material in ABAQUS with results obtained in MATLAB.

Figure 37: Third component of backstress vs. inelastic strain pathlength for CMSX-4, θ = 1000 ^{o}C: Comparison of the results obtained from User Material in ABAQUS with results obtained in MATLAB.

Figure 38: Instantaneous rate of energy storage vs. inelastic strain pathlength for CMSX-4 for loading along the <001> orientation, θ = 750 ^{o}C: Comparison of the results obtained from User Material in ABAQUS with results obtained in MATLAB.

Figure 39: Instantaneous rate of energy storage vs. inelastic strain pathlength for CMSX-4 for loading along the <001> orientation, θ = 982 ^{o}C: Comparison of the results obtained from User Material in ABAQUS with results obtained in MATLAB.

Figure 40: Instantaneous rate of energy storage vs. inelastic strain pathlength for CMSX-4 for loading along the <001> orientation, θ = 1000 ^{o}C: Comparison of the results obtained from User Material in ABAQUS with results obtained in MATLAB.

REFERENCES

[1] R. J. Asaro, "Micromechanics of cyrstals and polycrystals," *Advances in Applied Mechanics*, vol. 23, pp. 1-115, 1983.

[2] A. Bertram and J. Olschewski, "Anisotropic creep modelling of the single crystal superalloy SRR99," *Computational Materials Science*, vol. 5, pp. 12-16, 1996.

[3] B. A. Bilby, "Continous distribution of dislocations," in *Solid Mechanics*, I. Sneddon and R. Hill, Eds. Amsterdam: North-Hollands, 1960.

[4] S. B. Brown, K. H. Kim, and L. Anand, "An internal variable constitutive model for hotworking of metals," *International Journal of Plasticity*, vol. 5, pp. 95-130, 1989.

[5] P. Caron and T. Khan, "Improvement of creep strength in a Nickel-base single-crystal super-alloy by heat-treatment," *Materials Science and Engineering*, vol. 61, no. 2, pp. 173-184, 1983. 103

[6] P. Caron, T. Khan, and Y. G. Nakagawa, "Effect of orientation on the intermediate temperature creep behavior of Ni-base single crystal superalloys," *Scripta Metallurgica*, vol. 20, pp. 499-502, 1986.

[7] J. L. Chaboche, "Time-independent constitutive theories for cyclic plasticity," *International Journal of Plasticity*, vol. 2, no. 2, pp. 149-188, 1986.

[8] A. Coujou, M. Benyoucef, M. Legros, and N. Clement, "Role of the $\gamma - \gamma'$ interface on the mechanical properties of single crystals Nickel base superalloys," *Solid State Phenomena*, vol. 60, pp. 185-200, 1998.

[9] M. Durand-Charre, *The Microstructure of Superalloys*. Amsterdam: Gordon and Breach Science Publishers, 1997.

[10] B. F. Dyson, "Creep and fracture of metals: mechanisms and mechanics," *Revue de Physique Appliquee*, vol. 23, pp. 605-613, 1988.

[11] B. F. Dyson and M. Mclean, "Particle-coarsening, σ_o and tertiary creep," *Acta Metallurgica*, vol. 31, pp. 17-27, 1983.

[12] C. Eckart, "The thermodynamics of irreversible processes. iv. the theory of elasticity and anelasticity," *Physical Review*, vol. 73, pp. 373-382, 1948.

[13] J. D. Eshelby, "The continuum theory of lattice defects," in *Solid State Physics*, F. Seitz and D. Turnbull, Eds. New York: Academic Press, 1956.

[14] J. A. Ewing and W. Rosenhain, "The crystalling structure of metals," *Philosophical Transactions of the Royal Society, London. Series A*, vol. 193, pp. 353-375, 1920.

[15] R. N. Ghosh, R. V. Curtis, and M. Mclean, "Creep deformation of single crystal superalloys-modeling the crystallographic anisotropy," *Acta Metallurgica etMaterialia*, vol. 38, no. 10, pp. 1977-1992, Oct. 1990.

[16] R. N. Ghosh and M. Mclean, "Modeling the orientation dependence of tertiary creep in single crystal superalloy," *Scripta Metallurgica*, vol. 23, pp. 1301-1306, 1989.

[17] J. J. Gilman, *Micromechanics of Flow in Solids*. New York: McGraw-Hill, 1969.

[18] A. E. Green and P. M. Naghdi, "On thermodynamics and the nature of the second law," *Proceedings of the Royal Society of London Series A*, vol. 357, pp. 253-270, 1977.

[19] S. S. K. Gunturi, D. W. Maclachlan, and D. M. Knowles, "Anisotropic creep in CMSX-4 in orientations distant from <001>," *Materials Science and Engineering*, vol. A289, pp. 289-289, 2000.

[20] K. S. Havner, *Finite Plastic deformation of crystalline solids*. Cambridge: Cambridge University Press, 1992.

[21] P. J. Henderson and J. Lindblom, "High temperature creep in a <001> single crystal Nickel-base superalloy," *Scripta Materialia*, vol. 37, no. 4, pp. 491-496, 1997.

[22] M. Kamlah and P. Haupt, "On the macroscopic description of stored energy and self heating during plastic deformation," *International Journal of Plasticity*, vol. 13, no. 10, pp. 893-911, 1998.

[23] B. H. Kear and B. J. Piearcey, "Tensile and creep properties of single crystals of nickel-base superalloy MAR-M200," *Transactions of the Metallurgical Society of AIME*, vol. 239, no. 8, pp. 1209-1215, 1967.

[24] K. Kondo, "On the analytical and physical foundation of the theory of dislocations and yielding by the differential geometry of continua," *International Journal of Engineering Science*, vol. 2, pp. 219-251, 1964.

[25] E. KrÄoner, "Alleganeine kontinuumstheorie der verzetsmugen and eigenspannuugen," *Archive for Rational Mechanics and Analysis*, vol. 4, pp. 273-334, 1960.

[26] E. H. Lee, "Elastic-plastic deformation at finite strains," *Journal of Applied Mechanics*, vol. 36, pp. 1-6, 1969.

[27] G. R. Leverant and H. B. Kear, "The mechanism of creep in gamma prime precipitation-hardened nickel-base alloys at intermediate temperatures," *Metallurgical Transactions*, vol. 1, no. 2, pp. 491-498, 1970.

[28] G. R. Leverant, H. B. Kear, and J. M. Oblak, "Creep of precipitation-hardened Nickel-base alloy single-crystals at high-temperatures," *Metallurgical Transactions*, vol. 4, no. 1, pp. 335-362, 1973.

[29] R. A. MacKay and R. D. Maier, "The influence of orientation on the stress rupture properties of nickel-base superalloy single crystals," *Metallurgical Transactions A*, vol. 13A, pp. 1747-1754, 1982.

[30] D. W. Maclachlan and D. M. Knowles, "The effect of material behaviour on the analysis of single crystal turbine blades: Part I-material model," *Fatigue and Fracture of Engineering Materials and Structures*, vol. 25, pp. 385-398, 2002.

[31] J. J. Mason, A. J. Rosakis, and G. Ravichandran, "On the strain and strain rate dependence of the fraction of plastic work converted to heat: an experimental study using high speed infrared detectors and the Kolsky bar," *Mechanics of Materials*, vol. 17, pp. 135-145, 1994.

[32] N. Matan, D. C. Cox, P. Carter, M. A. Rist, C. M. F. Rae, and R. C. Reed, "Creep of CMSX-4 superalloy single crystals: Effects of misorientation and temperature," *Acta Materialia*, vol. 47, no. 5, pp. 1549-1563, 1999.

[33] M. McLean, *Directionally Solidified Materials for High Temperature Service*. London: The Metals Society, 1983.

[34] F. Mollica, K. R. Rajagopal, and A. R. Srinivasa, "The inelastic behavior of metals subject to loading reversal," *International Journal of Plasticity*, vol. 17, pp. 1119-1146, 2001.

[35] J. Murali Krishnan and K. R. Rajagopal, "Thermodynamic framework for the constitutive modeling of asphalt concrete: Theory and applications," *Journal of Materials in Civil Engineering*, vol. 16, no. 2, pp. 155-166, 2004.

[36] F. R. N. Nabarro, *Theory of Crystal Dislocations*. New York: Dover Publications, 1987.

[37] F. R. N. Nabarro, "The superiority of superalloys," *Materials Science and Engineering A*, vol. 184, no. 2, pp. 167-171, Aug. 1994.

[38] F. R. N. Nabarro, C. M. Cress, and P. Kotschy, "Thermodynamic driving force for rafting in superalloys," *Acta Materialia*, vol. 44, no. 8, pp. 3189-3198, Aug. 1996.

[39] F. R. N. Nabarro and H. L. De Villers, *The Physics of Creep*. London: Tylor & Francis, 1995.

[40] P. M. Naghdi and A. R. Srinivasa, "A dynamical theory of structured solids. i. Basic developments," *Philosophical Transactions of the Royal Society, London. Series A*, vol. 345, pp. 425-458, 1993.

[41] P. M. Naghdi and A. R. Srinivasa, "Characterization of dislocations and their influence on plastic deformation in single crystals," *International Journal of Engineering Science*, vol. 32, no. 7, pp. 1157-1182, Jul. 1994.

[42] D. W. Nicholson, "Large deformation theory of coupled thermoplasticity including kinematic hardening," *Acta Mechanica*, vol. 136, pp. 223-241, 1999.

[43] W. Noll, "On the foundations of the mechanics of continous media," Carnegie Institute of Technology, Department of Mathematics, Report Volume 17, 1957.

[44] G. R. Piercy, R. W. Cahn, and A. H. Cottrell, "A study of primary and conjugate ship in crystals of alpha-brass," *Acta Metallurgica*, vol. 3, pp. 332-338, 1955.

[45] G. R. Piercy, R. W. Cahn, and A. H. Cottrell, "Polyslip in polycrystals," *Acta Metallurgica*, vol. 6, pp. 85-94, 1958.

[46] T. M. Pollock and A. S. Argon, "Directional coarsening in Nickel-base single crystals with high volume fractions of coherent precipitates," *Acta Metallurgica et Materialia*, vol. 42, no. 6, pp. 1859-1874, 1994.

[47] S. C. Prasad, I. J. Rao, and K. R. Rajagopal, "A continuum model for the creep of single crystal nickel-base superalloys," *Acta Materialia*, vol. 53, no. 3, pp. 669-679, 2005.

[48] W. Qi and A. Bertram, "Damage modeling of the single crystal superalloy SRR99 under monotonous creep," *Computational Materials Science*, vol. 13, no. 4-5, pp. 132-141, 1998.

[49] K. R. Rajagopal, "Multiple configurations in continuum mechanics," Institute for Computational and Applied Mechanics, University of Pittsburgh, Pittsburgh, Pa, Report Volume 6, 1995.

[50] K. R. Rajagopal, "Art, craft and philosophy of modeling," In preperation.

[51] K. R. Rajagopal and N. Chandra, "A thermodynamic framework for the superplastic response of materials," *Materials Science Forum*, vol. 357, pp. 261-271, 2001.

[52] K. R. Rajagopal and A. R. Srinivasa, "On the inelastic behavior of solids-part i: Twinning," *International Journal of Plasticity*, vol. 11, pp. 653-678, 1995.

[53] K. R. Rajagopal and A. R. Srinivasa, "Inelastic behavior of materials-part ii: Energetics associated with discontinuous deformation twinning," *International Journal of Plasticity*, vol. 13, pp. 1-35, 1997.

[54] K. R. Rajagopal and A. R. Srinivasa, "Mechanics of the inelastic behavior of materials. part i. theoretical underpinnings," *International Journal of Plasticity*, vol. 14, pp. 945-967, 1998.

[55] K. R. Rajagopal and A. R. Srinivasa, "Mechanics of the inelastic behavior of materials. part ii. inelastic response." *International Journal of Plasticity*, vol. 14, pp. 969-995, 1998.

[56] K. R. Rajagopal and A. R. Srinivasa, "On the thermodynamics of shape memory wires," *International Journal of Plasticity*, vol. 50, pp. 459-496, 1999.

[57] K. R. Rajagopal and A. R. Srinivasa, "A thermodynamic framework for rate type fluid models," *Journal of Non-Newtonian Fluid Mechanics*, vol. 88, pp. 207-227, 2000.

[58] K. R. Rajagopal and A. R. Srinivasa, "Modeling anisotropic fluids within the framework of bodies with multiple natural configurations," *Journal of Non-Newtonian Fluid Mechanics*, vol. 99, pp. 109-124, 2001.

[59] K. R. Rajagopal and A. R. Srinivasa, "On the thermomechanics of materials that have multiple natural configurations. part i: Viscoelasticity and classical plasticity," *Zeitschrift Fur Angewandte Mathematik Und Physik*, vol. 55, pp. 861-893, 2004.

[60] K. R. Rajagopal and A. R. Srinivasa, "On the thermomechanics of materials that have multiple natural configurations. part ii: Twinning and solid to solid phase transformation," *Zeitschrift Fur Angewandte Mathematik Und Physik*, vol. 55, pp. 1074-1093, 2004.

[61] K. R. Rajagopal and A. S. Wineman, "A constitutive equation for non-linear solids which undergo deformation induced microstructural changes," *International Journal of Plasticity*, vol. 8, pp. 385-395, 1992.

[62] I. J. Rao, J. D. Humphrey, and K. R. Rajagopal, "Biological growth and remodeling: A uniaxial example with application to tendon and ligaments," *CMES-Computer Modeling in Engineering & Sciences*, vol. 4, no. 3-4, pp. 439-455, Jun. 2003.

[63] I. J. Rao and K. R. Rajagopal, "Thermomechanical framework for the crystallization of polymers," *Zeitschrift Fur Angewandte Mathematik Und Physik*, vol. 53, pp. 365-406, 2002.

[64] R. C. Reed, N. Matan, D. C. Cox, M. A. Rist, and C. M. F. Rae, "Creep of CMSX-4 superalloy single crystals: Effects of rafting at high temperature," *Acta Materialia*, vol. 47, no. 12, pp. 3367-3381, 1999.

[65] R. E. Reed-Hill and R. Abbaschian, *Physical Metallurgy Principles*. Boston: PWS-KENT, 1992.

[66] V. Sass, U. Glatzel, and M. Feller-Kniepmeier, "Creep anisotropy in the monocrystalline Nickel-base superalloy CMSX-4," in *Superalloys 1996*, R. D. Kissinger, D. J. Deye, D. L. Anton, A. D. Cetel, M. V. Nathal, T. M. Pollock, and D. A. Woodford, Eds. Warrendale, PA: The Minerals, Metals and Materials Society, 1996, pp. 283-290.

[67] F. Schubert, G. Fleury, and T. Steinhaus, "Modeling of the mechanical behavior of the single-crystal turbine alloy CMSX-4 during thermomechanical loading," *Modelling and Simulation in Materials Science and Engineering*, vol. 8, pp. 947-957, 2000.

[68] S. Socrate and D. M. Parks, "Numerical determination of the elastic driving force for directional coarsening in Ni-superalloys," *Acta Metallurgica et Materialia*, vol. 41, no. 7, pp. 2185-2209, Jul. 1993.

[69] J. Svoboda and P. Lukas, "Model of creep in <001>-oriented superalloy single crystals," *Acta Materialia*, vol. 46, no. 10, pp. 3421-3431, 1998.

[70] G. I. Taylor, "The mechanisms of plastic deformation of crystals," *Philosophical Transactions of the Royal Society, London. Series A*, vol. 145, pp. 362-387, 1926.

[71] G. I. Taylor and C. F. Elam, "The distortion of an aluminum crystal during tensile test," *Philosophical Transactions of the Royal Society, London. Series A*, vol. 102, pp. 643-667, 1923.

[72] G. I. Taylor and C. F. Elam, "The plastic extension and fracture of aluminum crystals," *Philosophical Transactions of the Royal Society, London. Series A*, vol. 108, pp. 28-51, 1925.

[73] G. I. Taylor and C. F. Elam, "The distortion of iron crystals," *Philosophical Transactions of the Royal Society, London. Series A*, vol. 112, pp. 337-361, 1926.

[74] C. Truesdell and W. Noll, *The Non-Linear Field Theories of Mechanics*, 1st ed. Berlin: Springer-Verlag, 1965.

[75] M. Veron, Y. Brechet, and F. Louchet, "Directional coarsening of Ni-based superalloys: Computer simulation at the mesoscopic level," *Acta Materialia*, vol. 44, no. 9, pp. 3633-3641, Sep. 1996.

[76] R. O. Williams, "Stored energy and release kinetics in Lead, Aluminum, Silver, Nickel, Iron and Zirconium after deformation," *Transactions of the Metallurgical Society of AIME*, vol. 224, pp. 719-726, 1962.

[77] A. S. Wineman and K. R. Rajagopal, "On constitutive theory for materials undergoing microstructural changes," *Archives of Mechanics*, vol. 42, pp. 53-75, 1990.
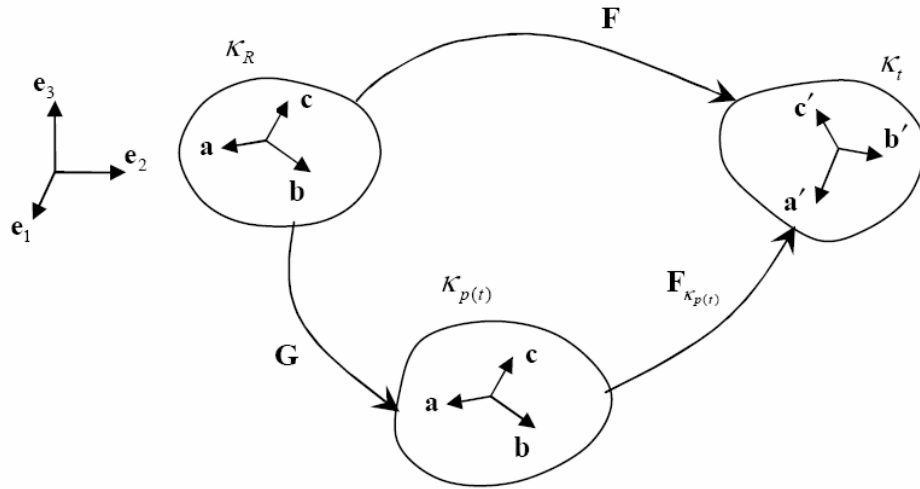
Fig. 1. Natural configurations associated with the body.
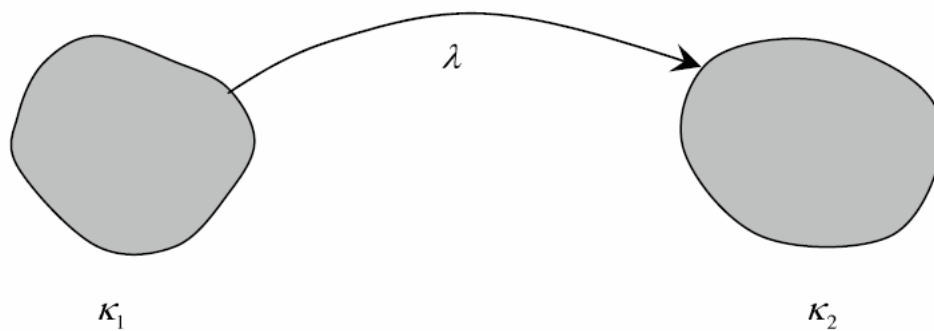
Fig. 2. Noll's rule for simple materials.
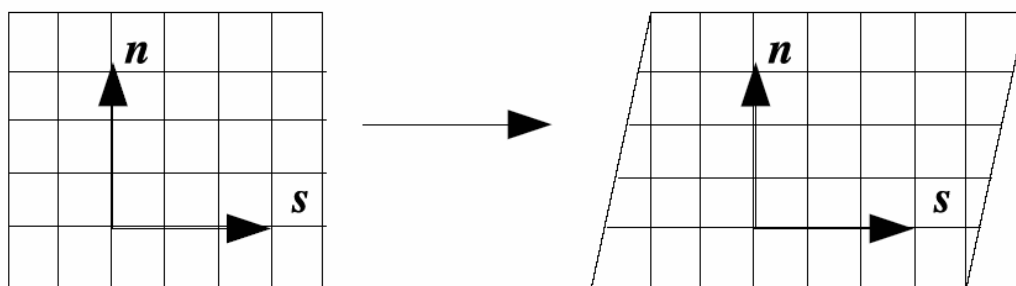
Fig. 3. Shearing of the lattice of a single crystal.
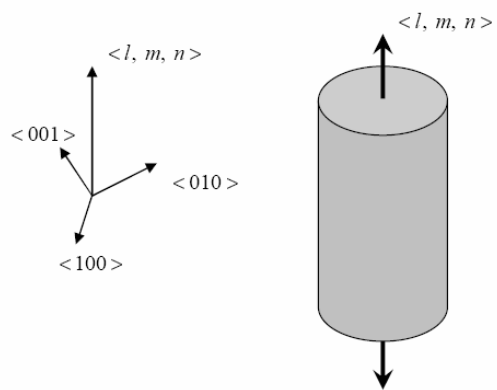
Fig. 4. Creep of a specimen loaded along the direction $<l, m, n>$ under constant load.
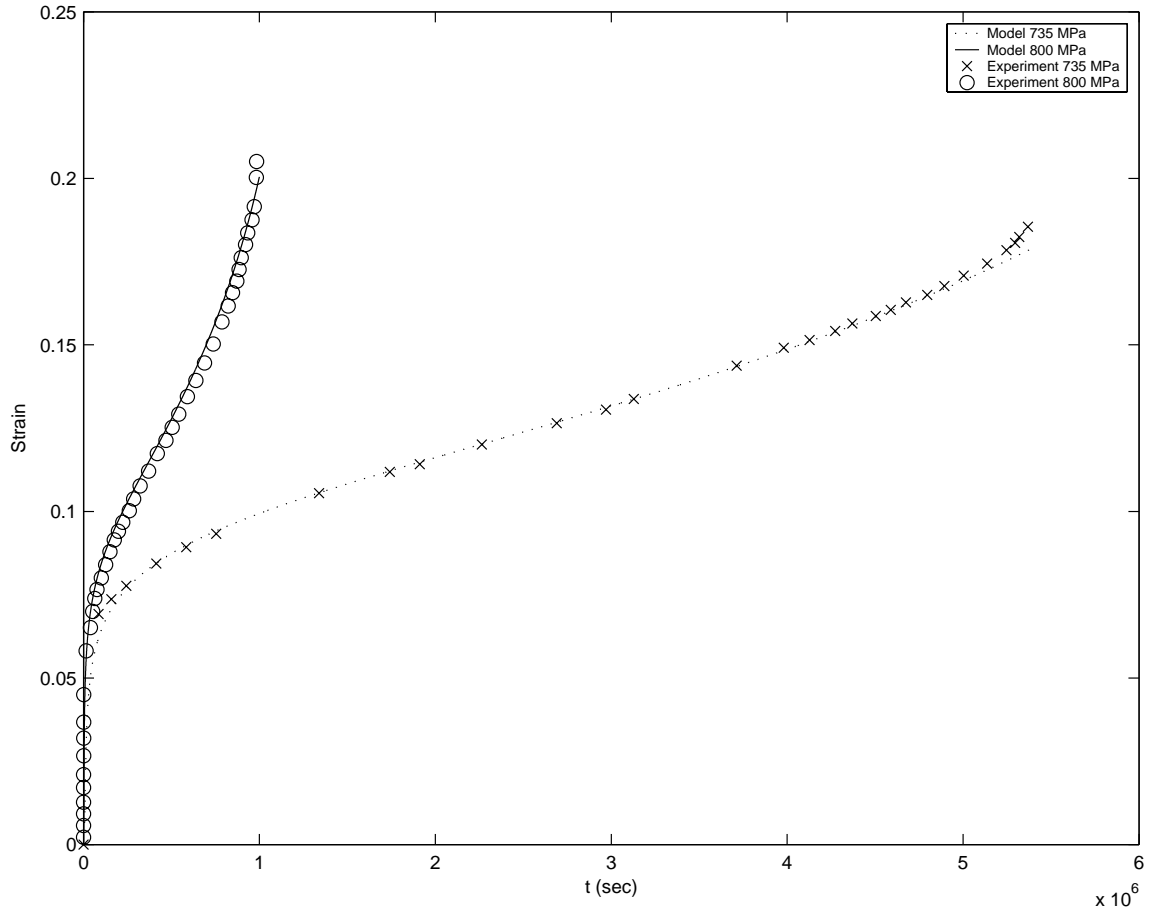
Fig. 5. Strain vs. time for CMSX-4 for loading along the <001> orientation, θ = 750 ^{o}C: Comparison of the predictions of the model with experimental results of Svoboda and Lucas [69] and Henderson and Lindblom [21].
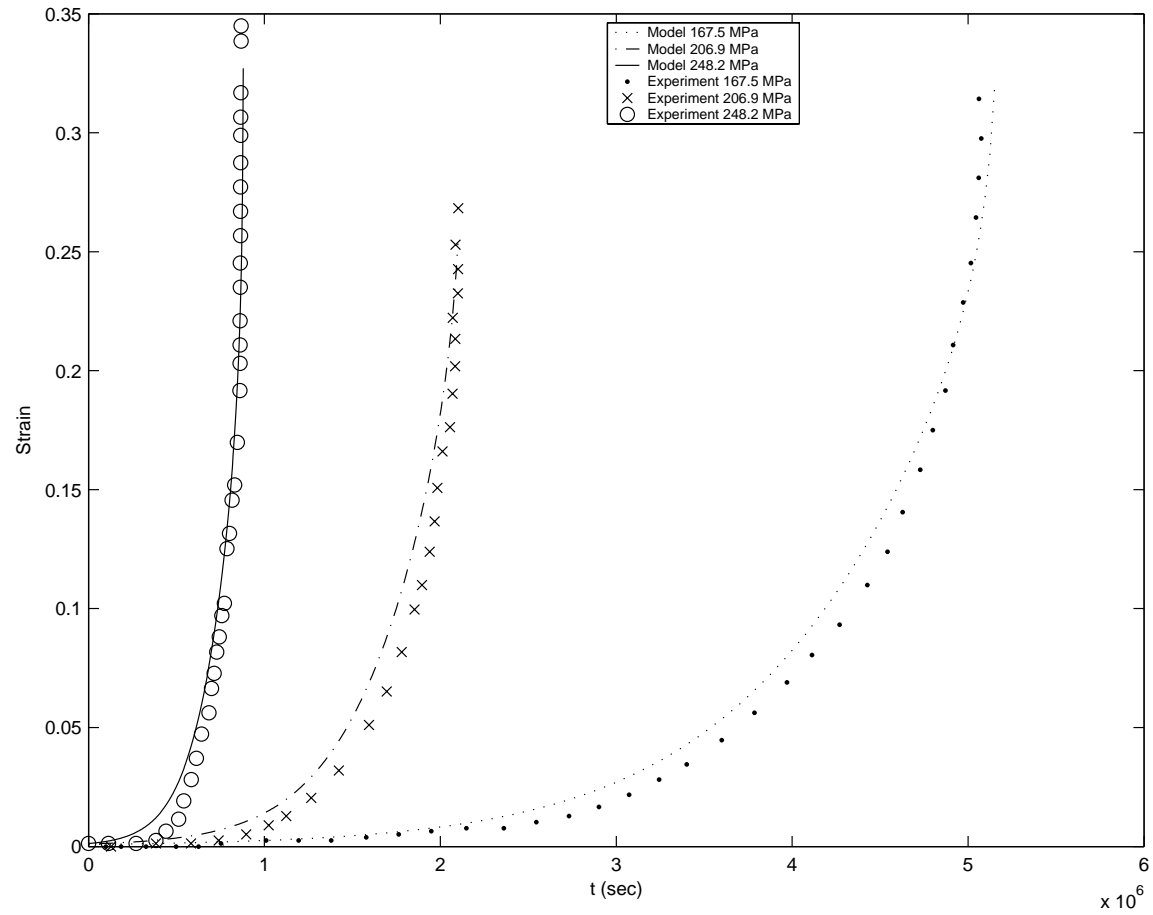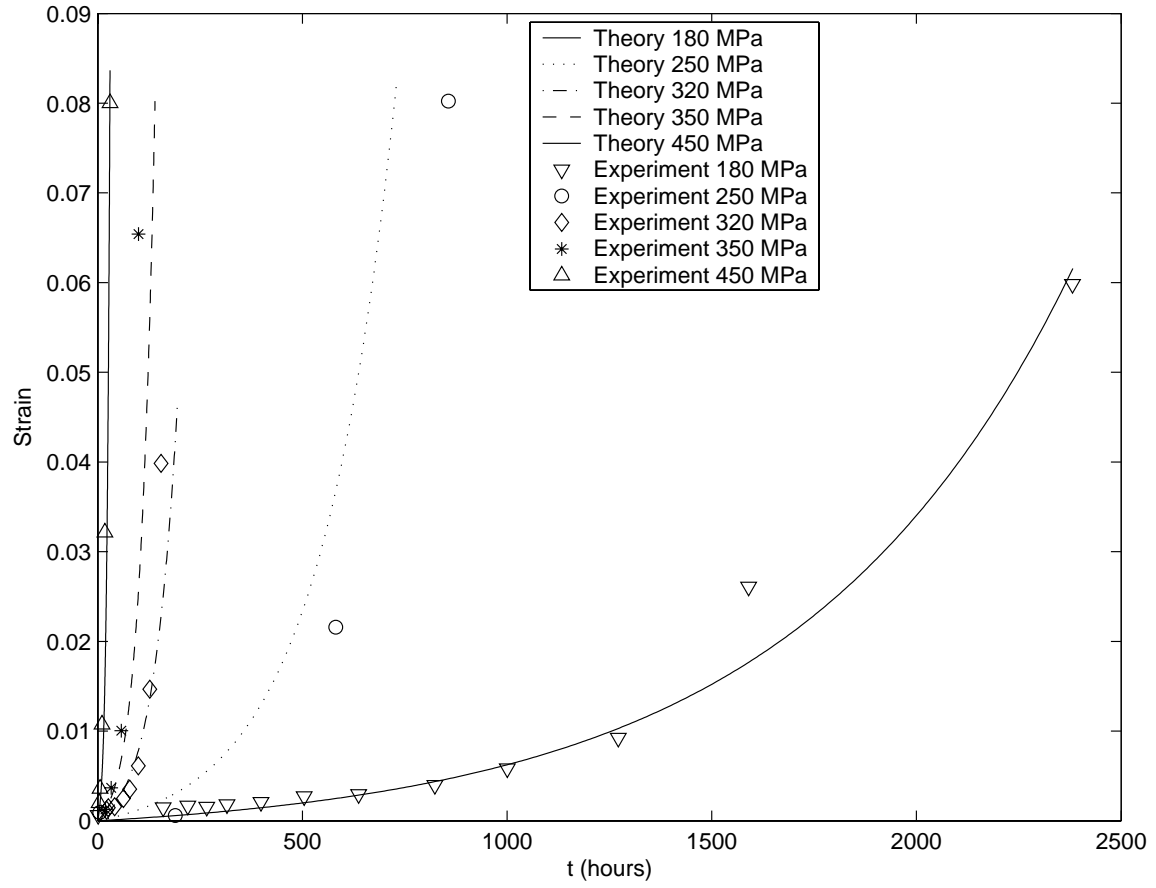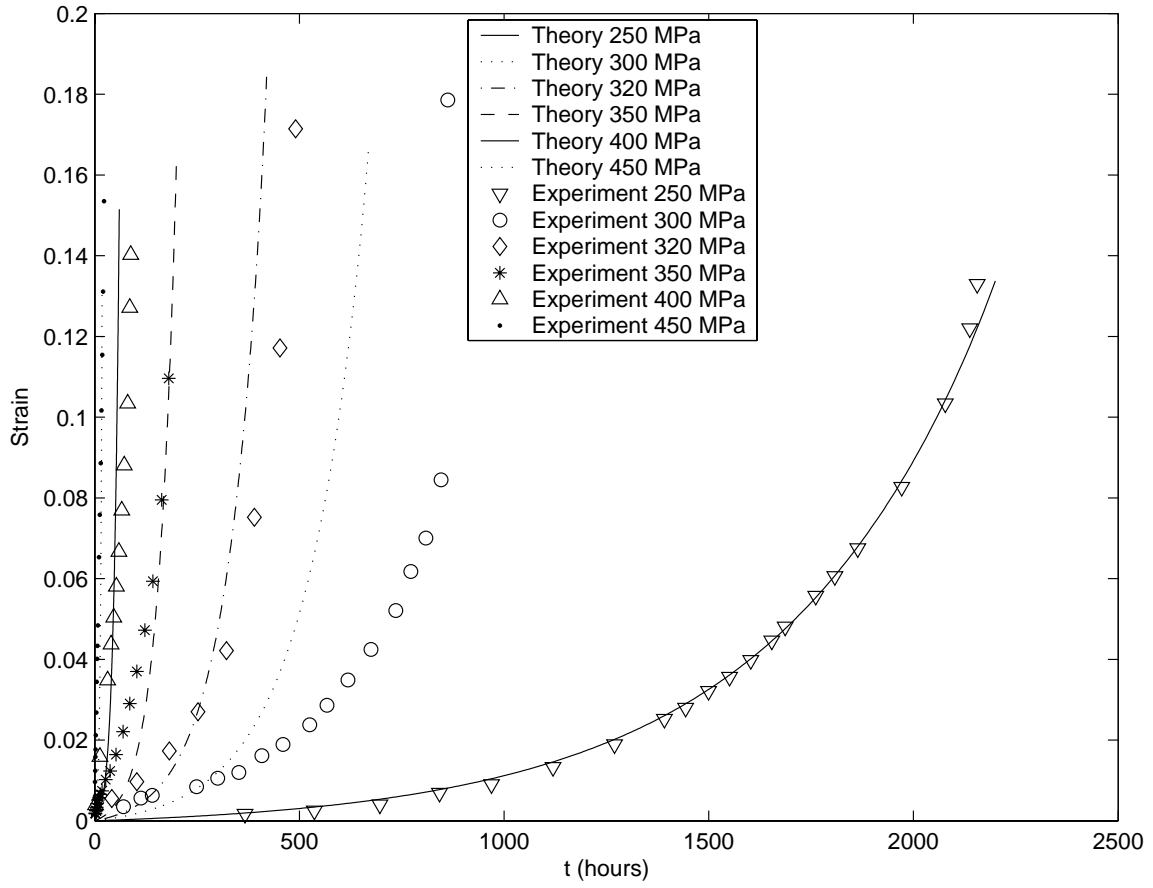
Fig. 6. Strain vs. time for CMSX-4 for loading along the <001> orientation, θ = 982 ^oC: Comparison of the predictions of the model with experimental results of Svoboda and Lucas [69] and Henderson and Lindblom [21].
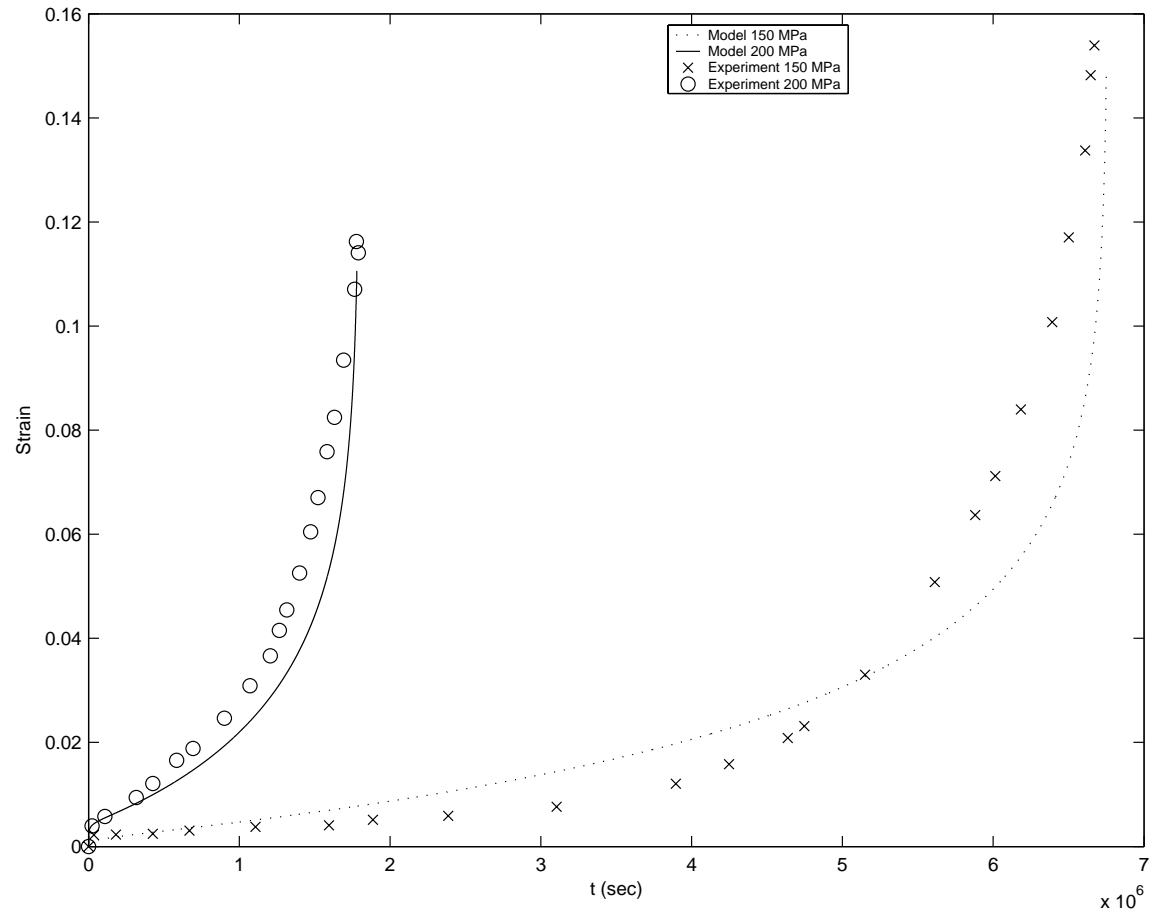
Fig. 7. Strain vs. time for CMSX-4 for loading along the <001> orientation, $\theta = 1000\ ^oC$: Comparison of the predictions of the model with experimental results of Svoboda and Lucas [69] and Henderson and Lindblom [21].
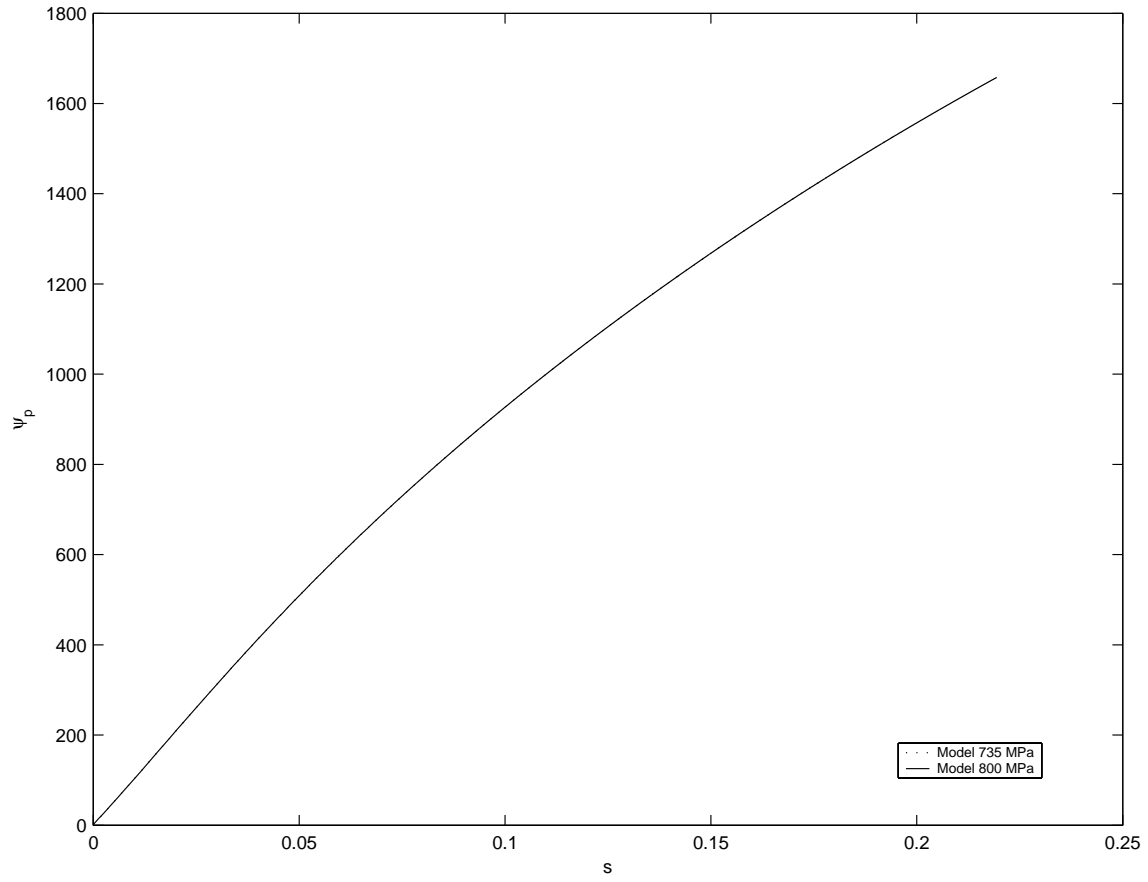
Fig. 8. Inelastic stored energy vs. inelastic strain pathlength for CMSX-4 for loading along the <001> orientation, $\theta = 750\ ^{o}$C: Predictions of the model.
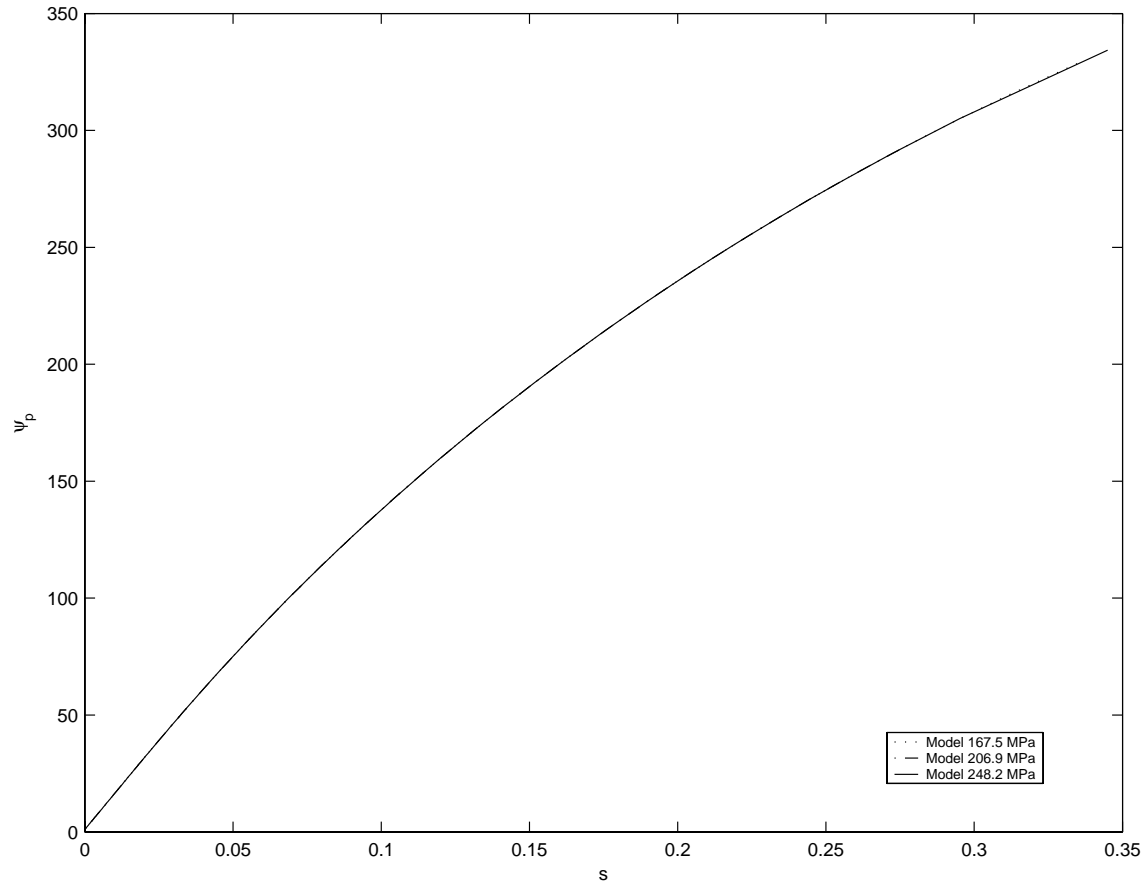
Fig. 9. Inelastic stored energy vs. inelastic strain pathlength for CMSX-4 for loading along the <001> orientation, $\theta = 982 \ ^{o}C$: Predictions of the model.
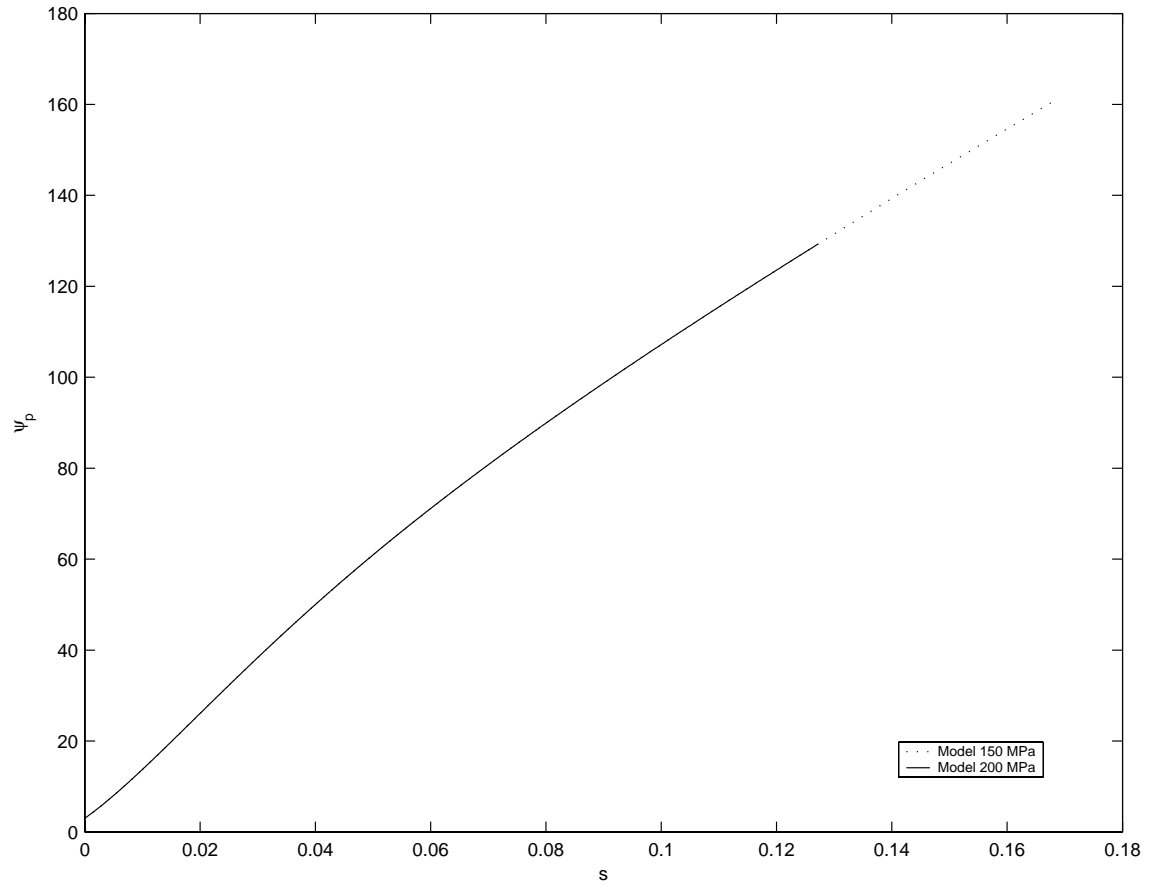
Fig. 10. Inelastic stored energy vs. inelastic strain pathlength for CMSX-4 for loading along the <001> orientation, $\theta = 1000\ ^{o}C$: Predictions of the model.
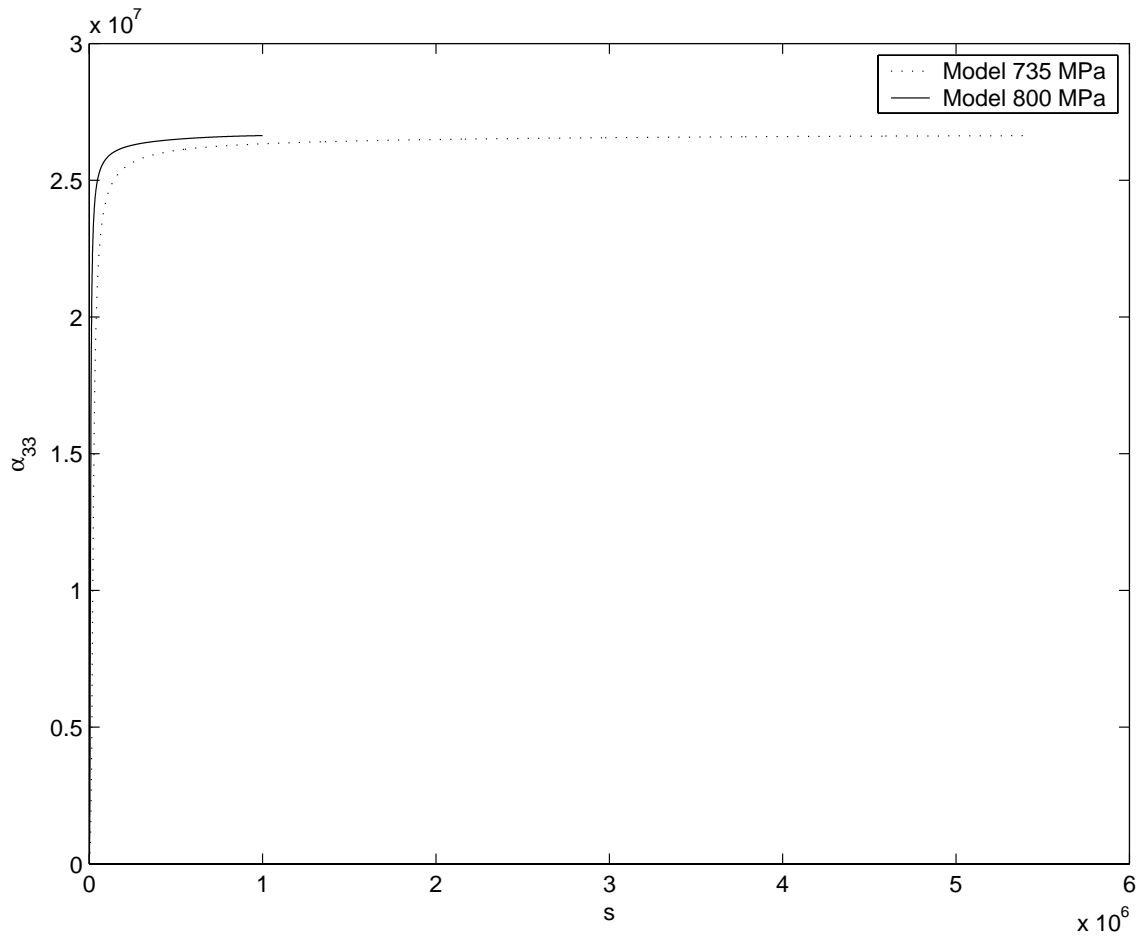
Fig. 11. Third component of backstress vs. inelastic strain pathlength for CMSX-4 for loading along the <001> orientation, $\theta = 750\ ^{o}$C: Predictions of the model.
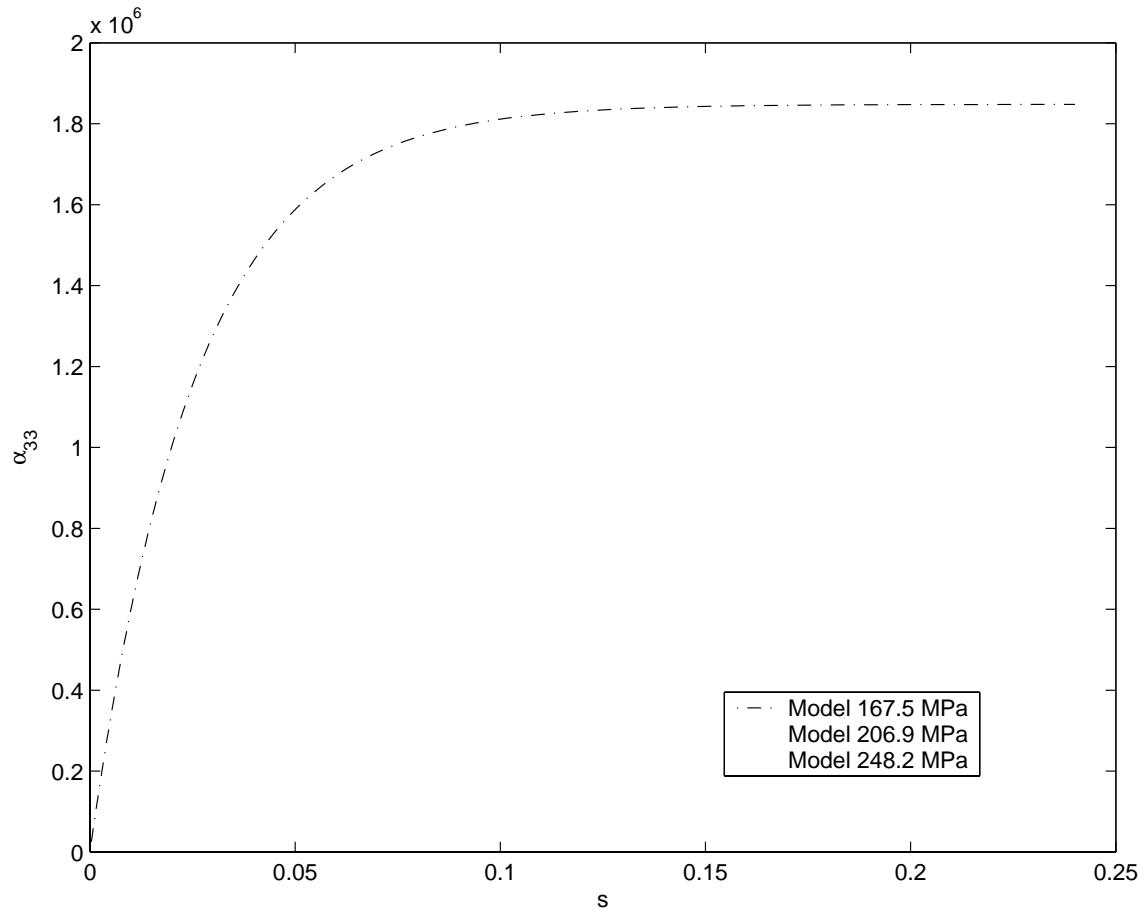
Fig. 12. Third component of backstress vs. inelastic strain pathlength for CMSX-4 for loading along the <001> orientation, $\theta = 982\ ^oC$: Predictions of the model.
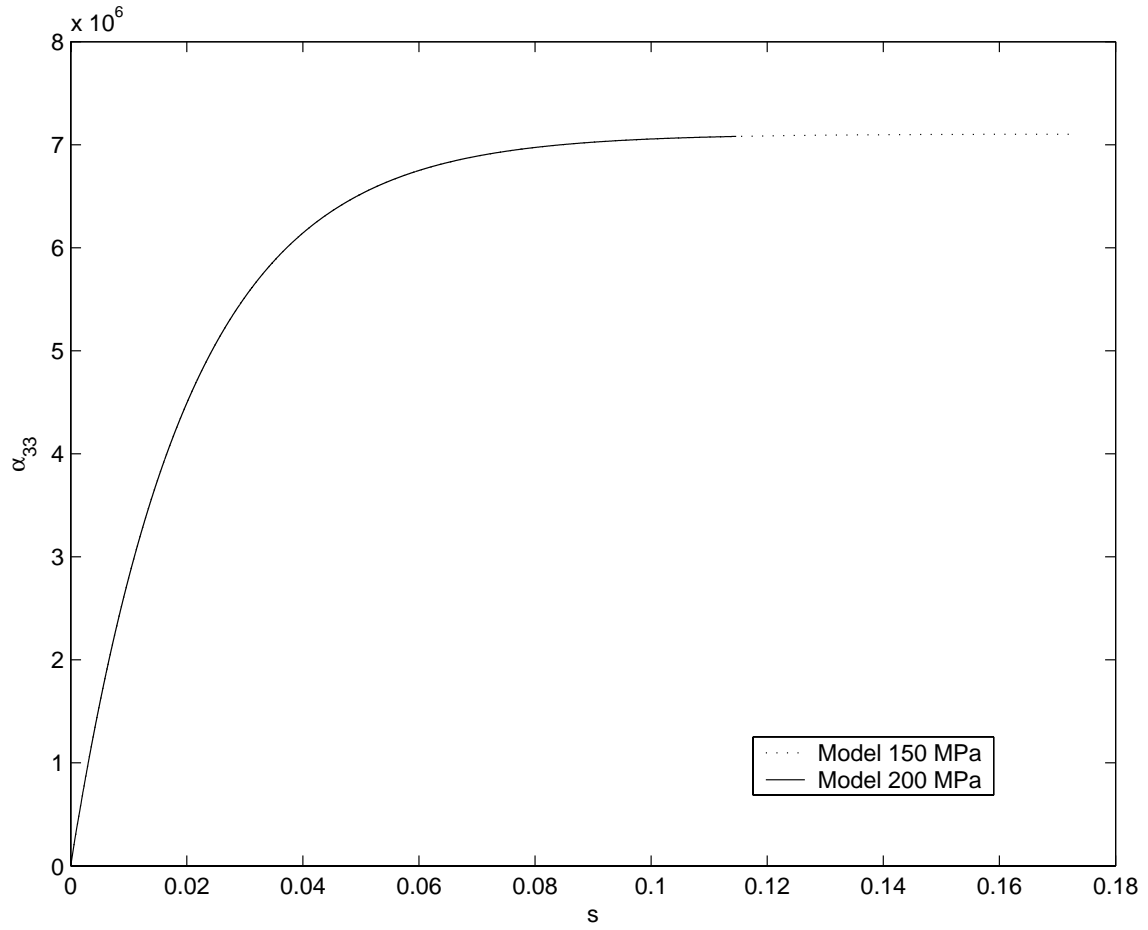
Fig. 13. Third component of backstress vs. inelastic strain pathlength for CMSX-4 for loading along the <001> orientation, $\theta = 1000\ ^{o}$C: Predictions of the model.
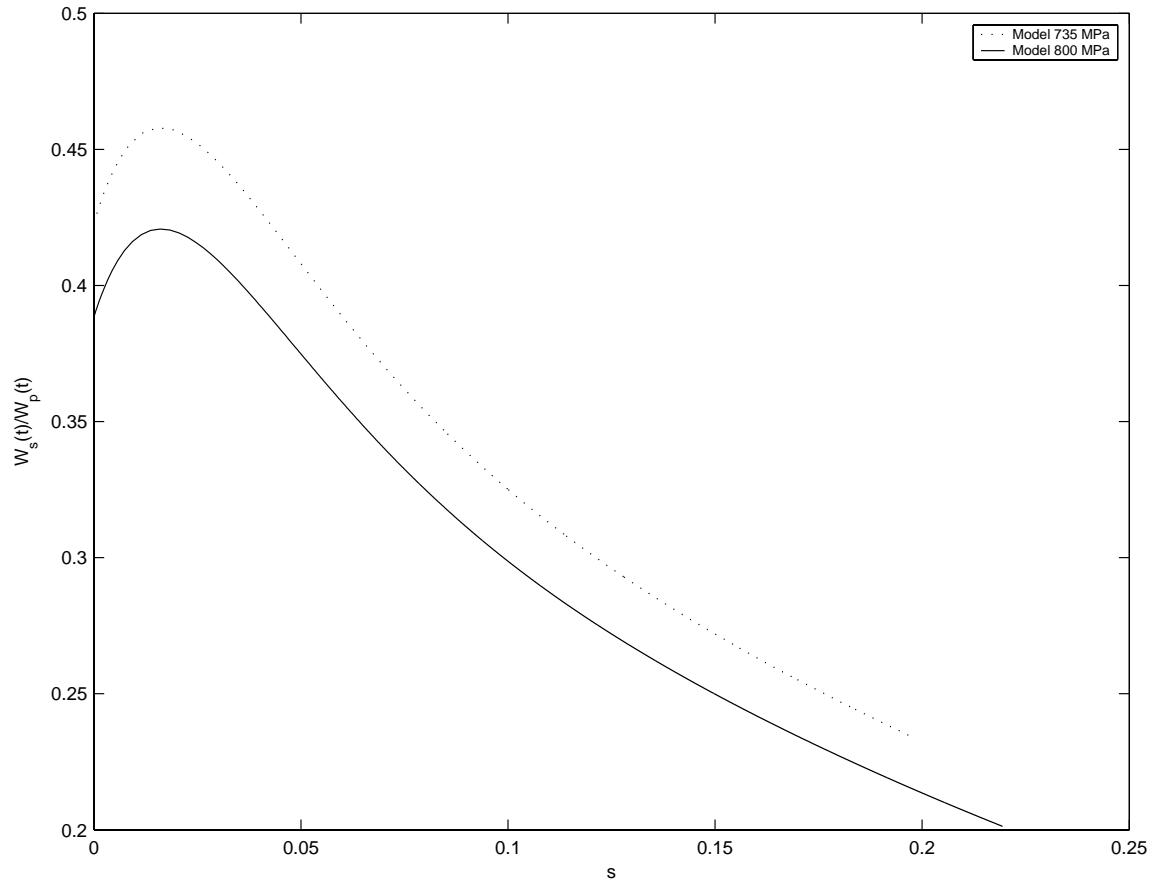
Fig. 14. Instantaneous rate of energy storage vs. inelastic strain pathlength for CMSX-4 for loading along the <001> orientation, $\theta = 750\ {}^{o}\mathrm{C}$: Predictions of the model.
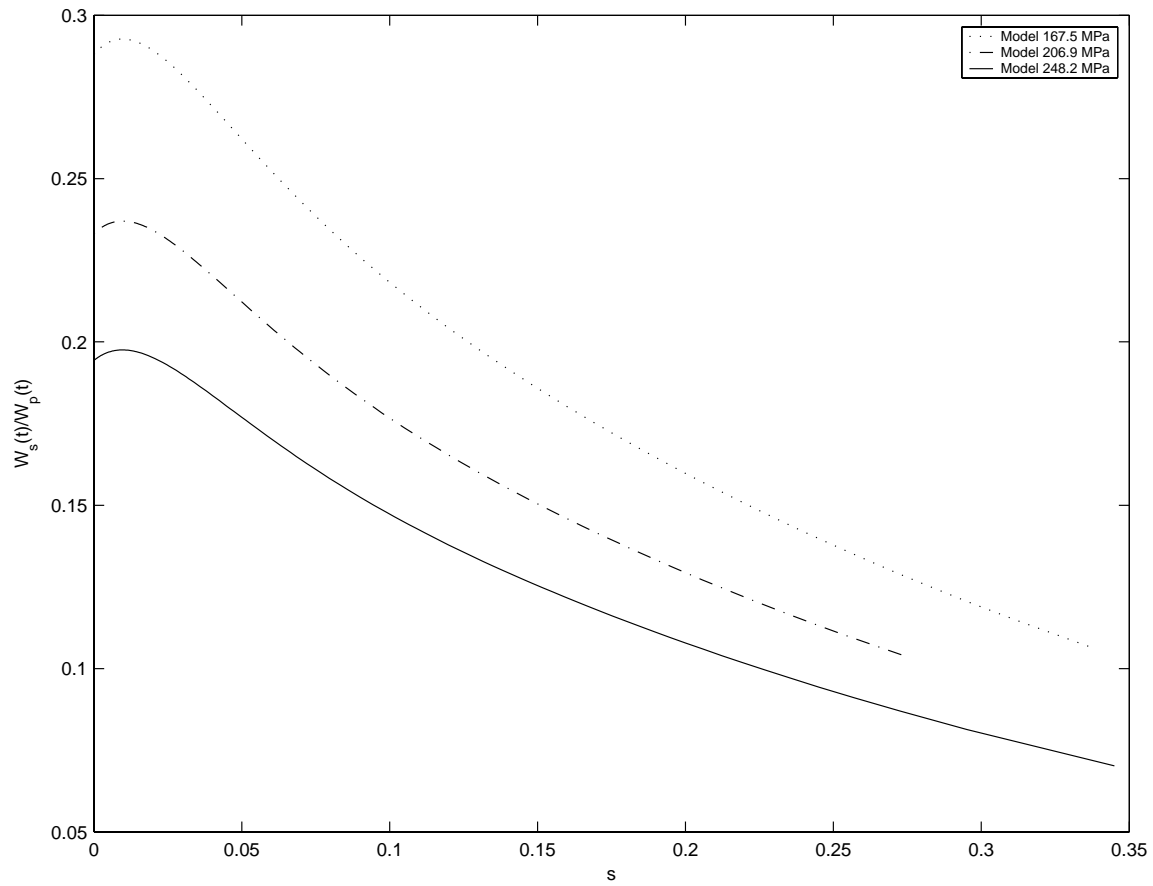
Fig. 15. Instantaneous rate of energy storage vs. inelastic strain pathlength for CMSX-4 for loading along the <001> orientation, $\mu = 982$ oC: Predictions of the model.
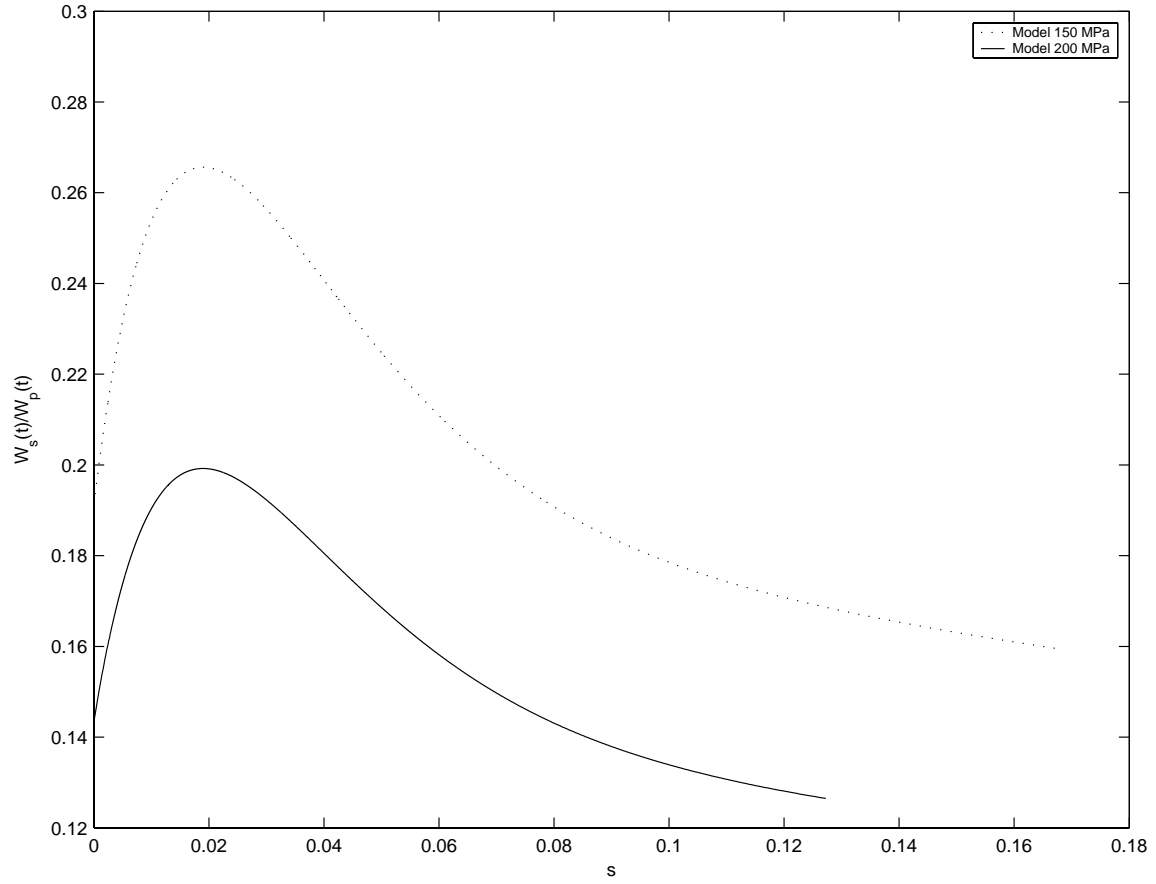
Fig. 16. Instantaneous rate of energy storage vs. inelastic strain pathlength for CMSX-4 for loading along the <001> orientation, $\theta = 1000$ ^{o}C: Predictions of the model.
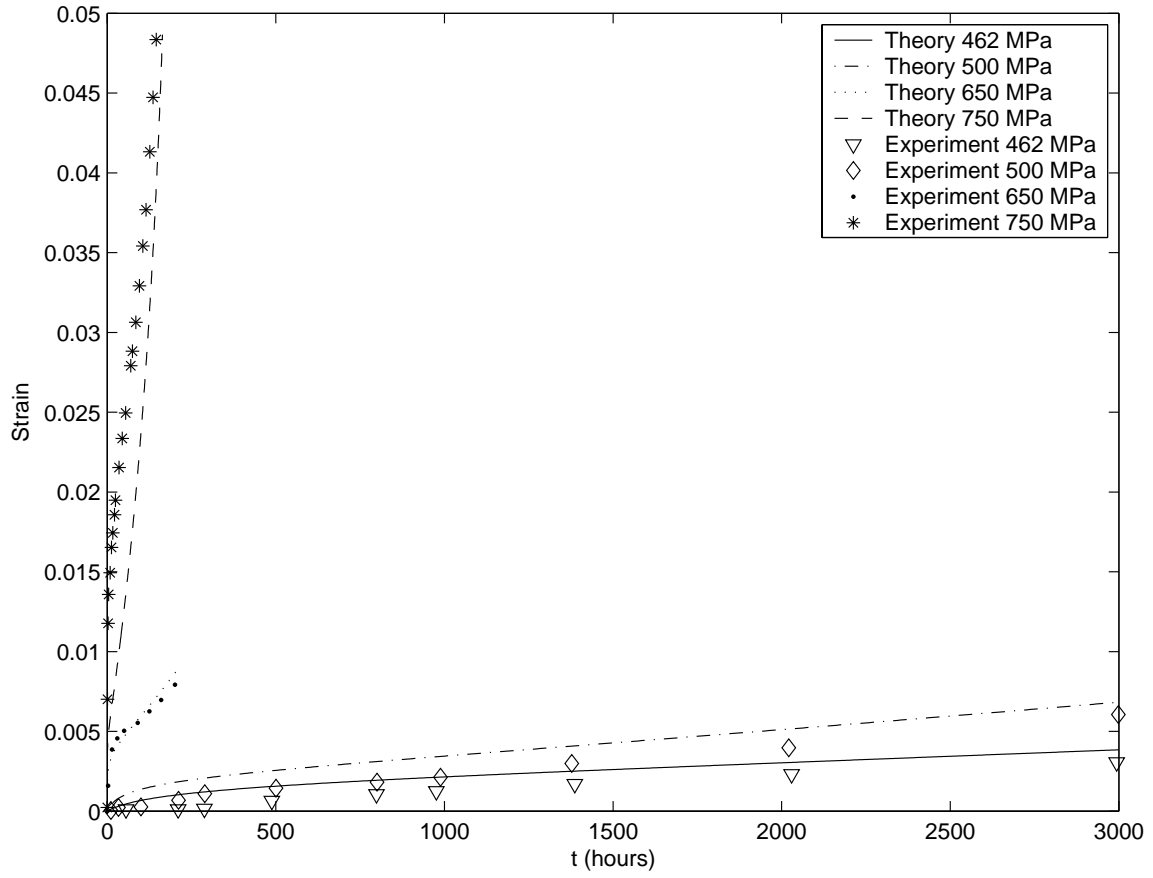
Fig. 17. Strain vs. time for CMSX-4 for loading along the <001> orientation, θ = 800 ^{o}C: Comparison of the predictions of the model with experimental results of Schubert et al., [67].
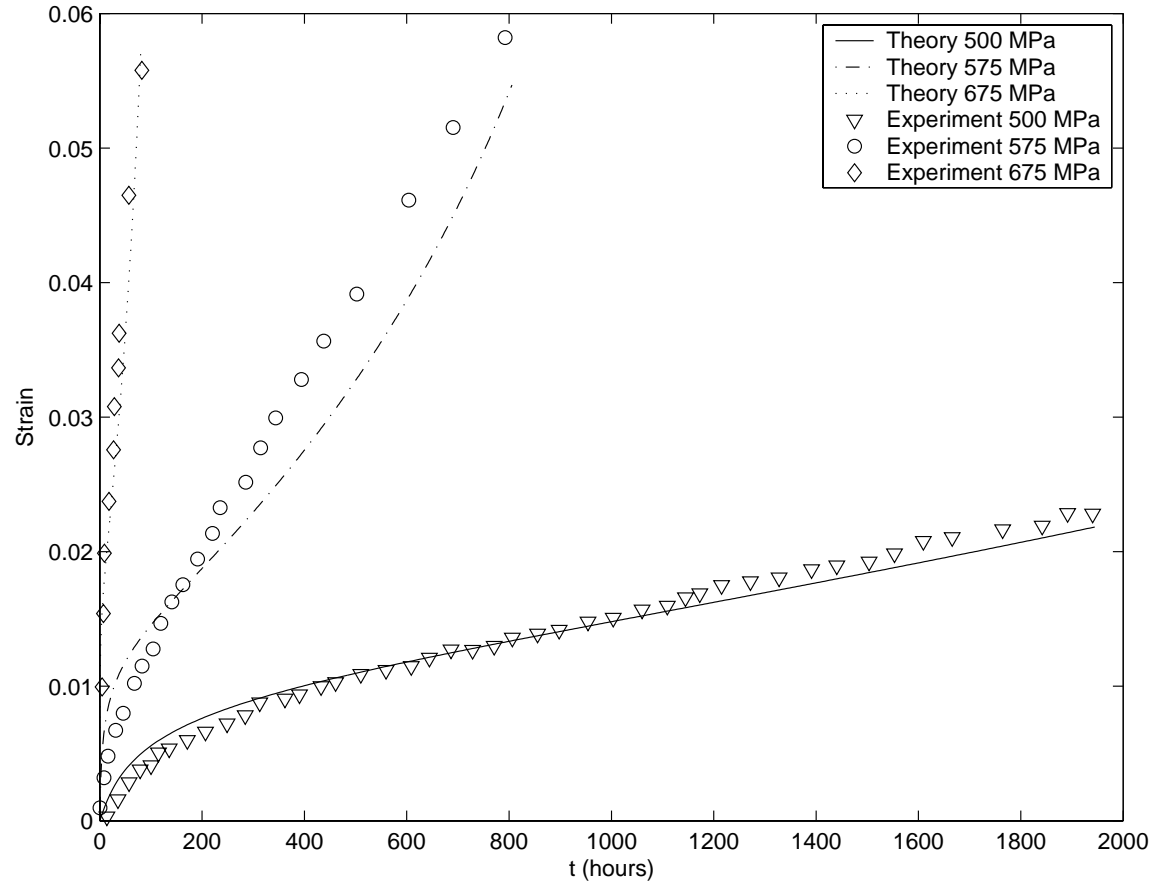
Fig. 18. Strain vs. time for CMSX-4 for loading along the <111> orientation, θ = 800 ^{o}C: Comparison of the predictions of the model with experimental results of Schubert et al., [67].
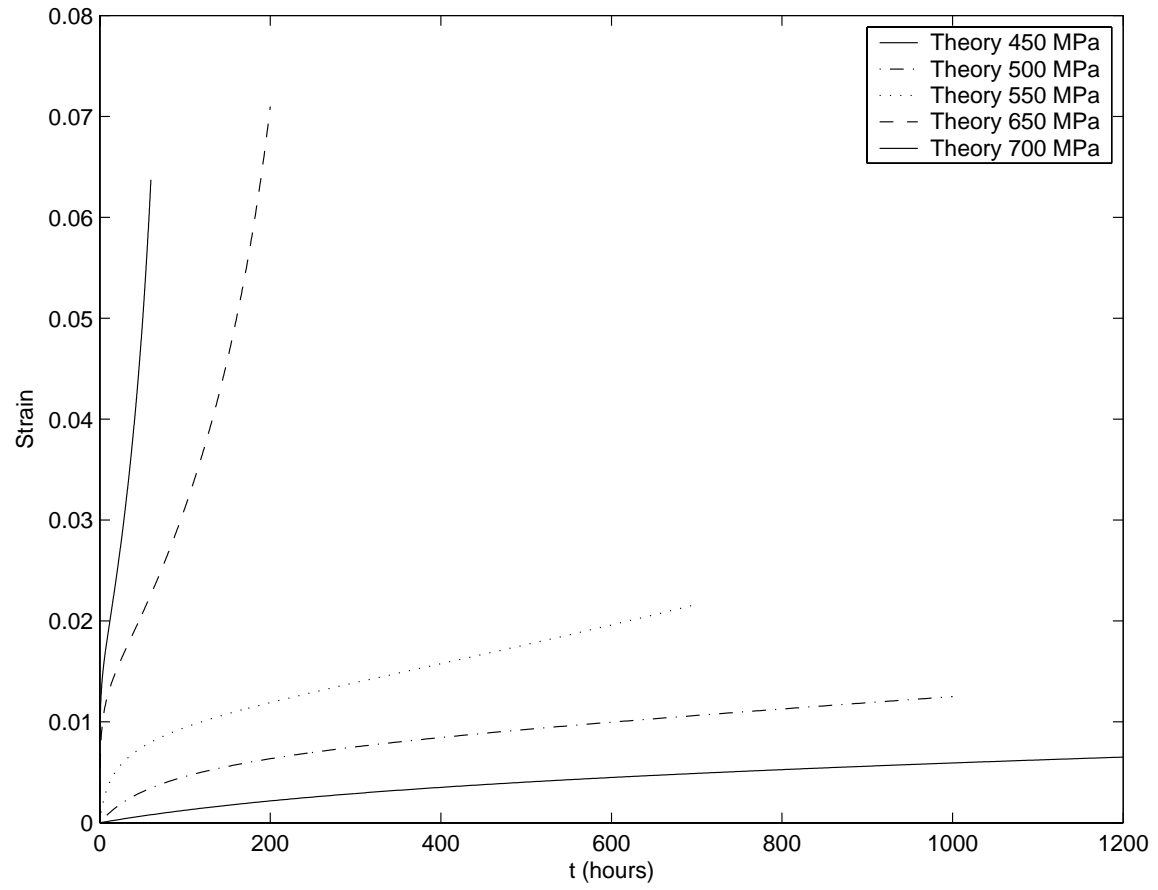
Fig. 19. Strain vs. time for CMSX-4 for loading along the <011> orientation, θ = 800 ^{o}C: Predictions of the model.

Fig. 20. Strain vs. time for CMSX-4 for loading along the <001> orientation, $\theta = 950\ ^oC$: Comparison of the predictions of the model with experimental results of MacLachlan et al., [30].

Fig. 21. Strain vs. time for CMSX-4 for loading along the <111> orientation, θ = 950 ^{o}C: Comparison of the predictions of the model with experimental results of MacLachlan et al., [30].
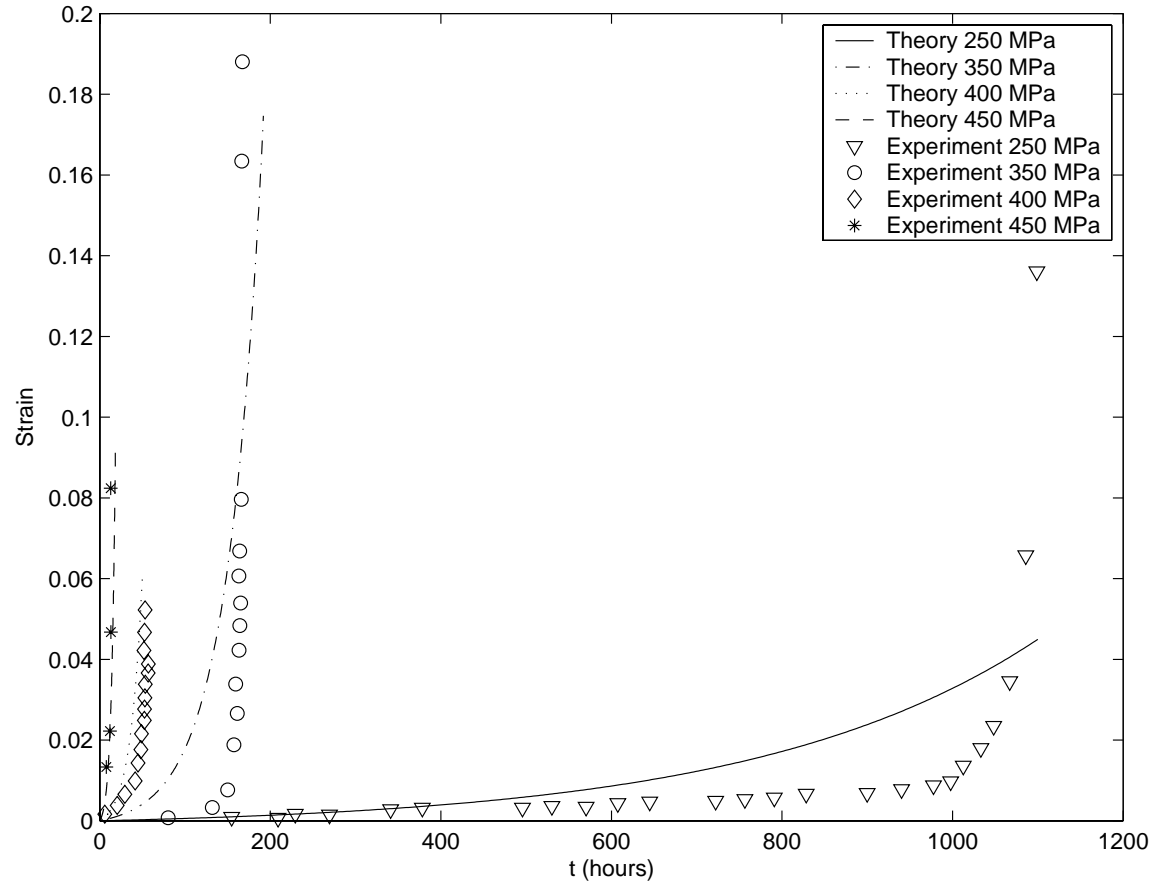
Fig. 22. Strain vs. time for CMSX-4 for loading along the <011> orientation, θ = 950 ^{o}C: Comparison of the predictions of the model with experimental results of MacLachlan et al., [30].
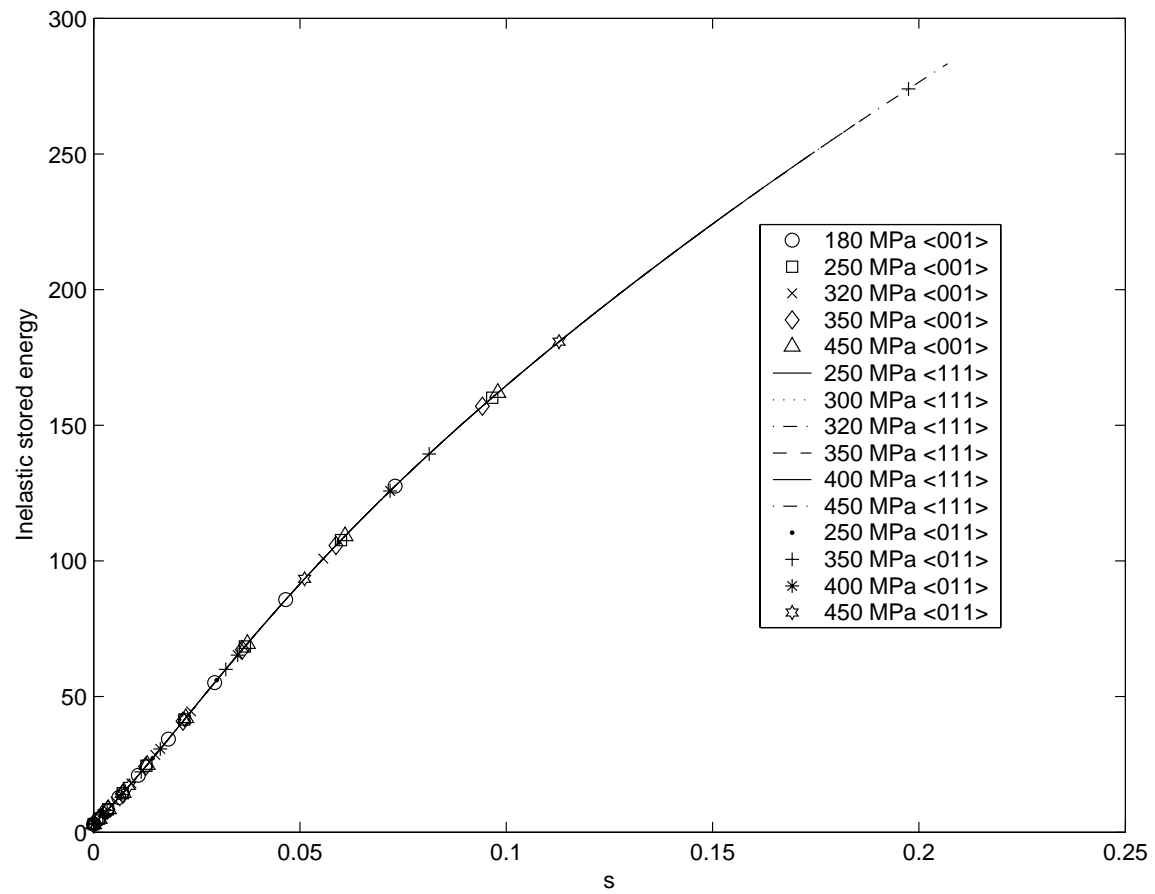
Fig. 23. Inelastic stored energy vs. inelastic strain pathlength for CMSX-4 , θ = 800 ^{o}C: Predictions of the model.
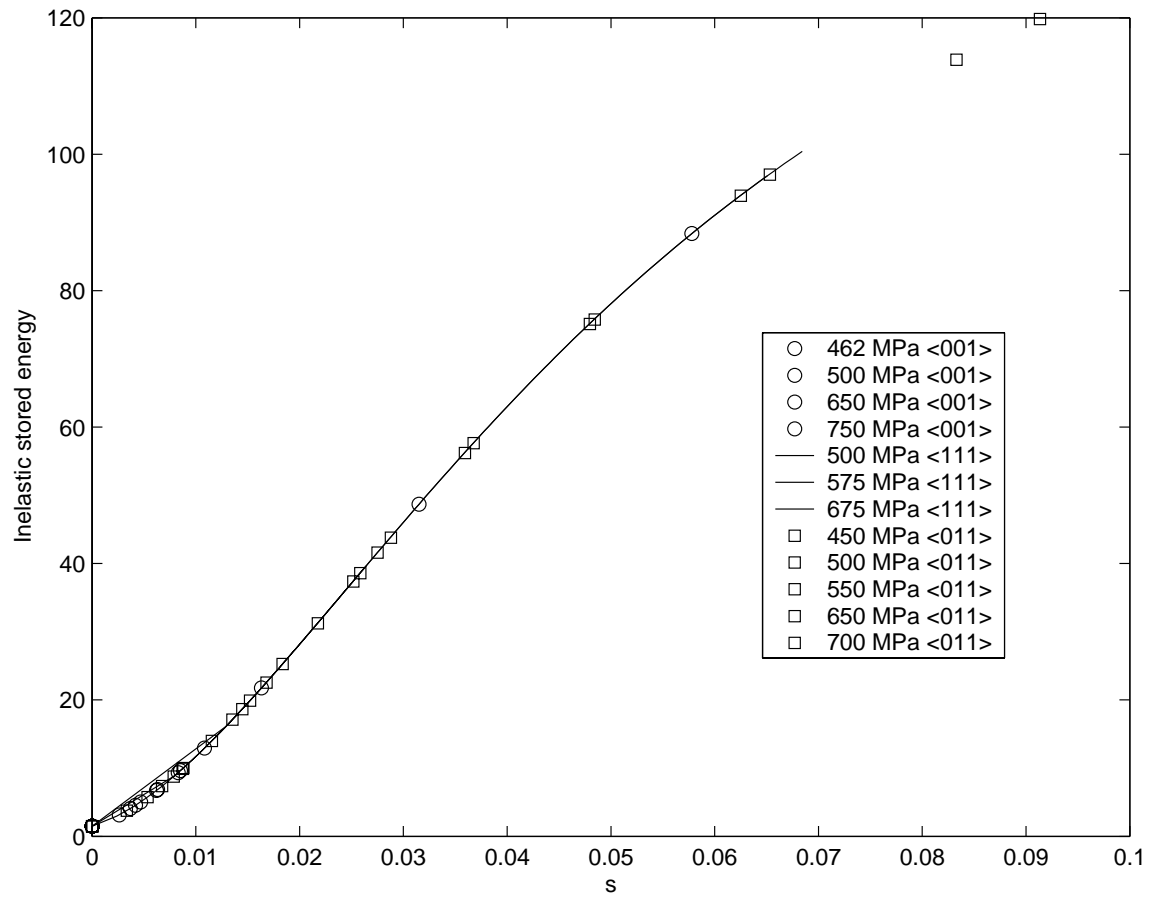
Fig. 24. Inelastic stored energy vs. inelastic strain pathlength for CMSX-4 , θ = 950 ^{o}C: Predictions of the model.
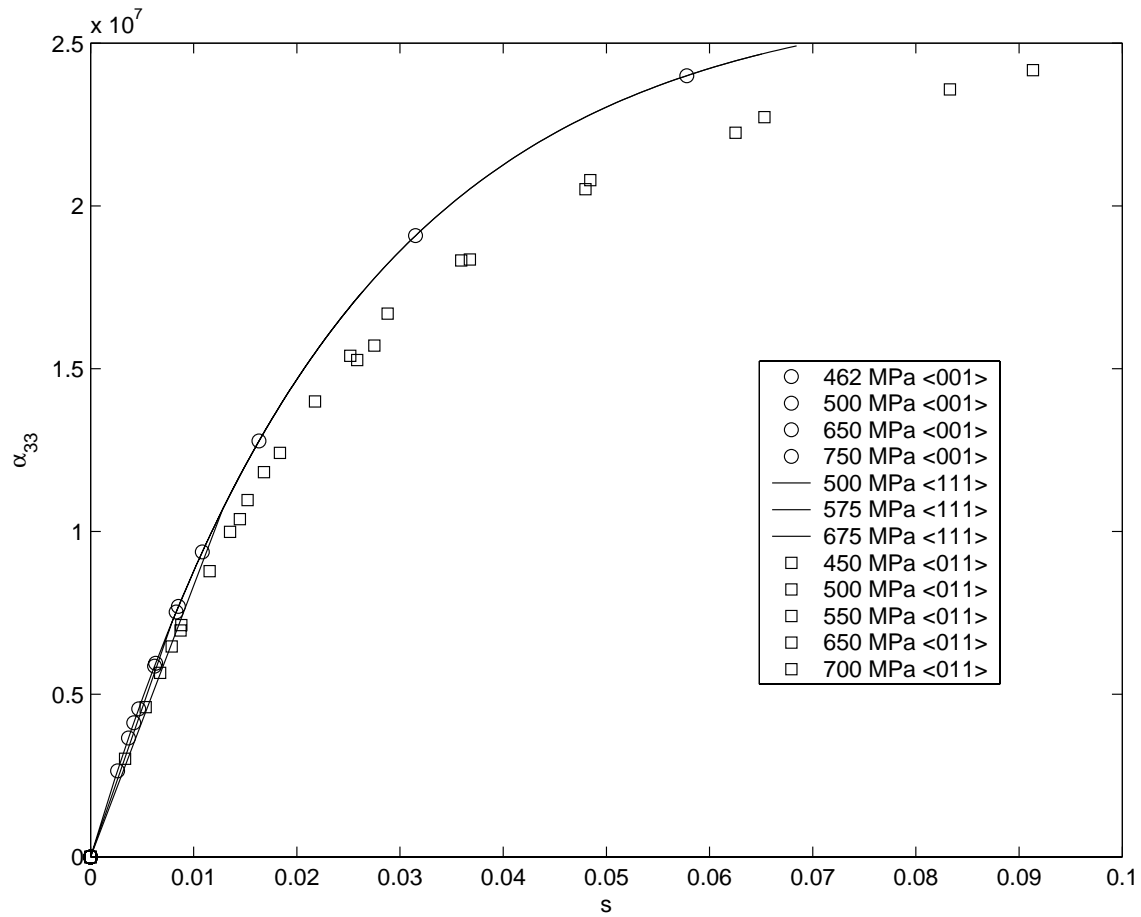
Fig. 25. Third component of backstress vs. inelastic strain pathlength for CMSX-4 , $\theta = 800\ {}^{o}C$: Predictions of the model.
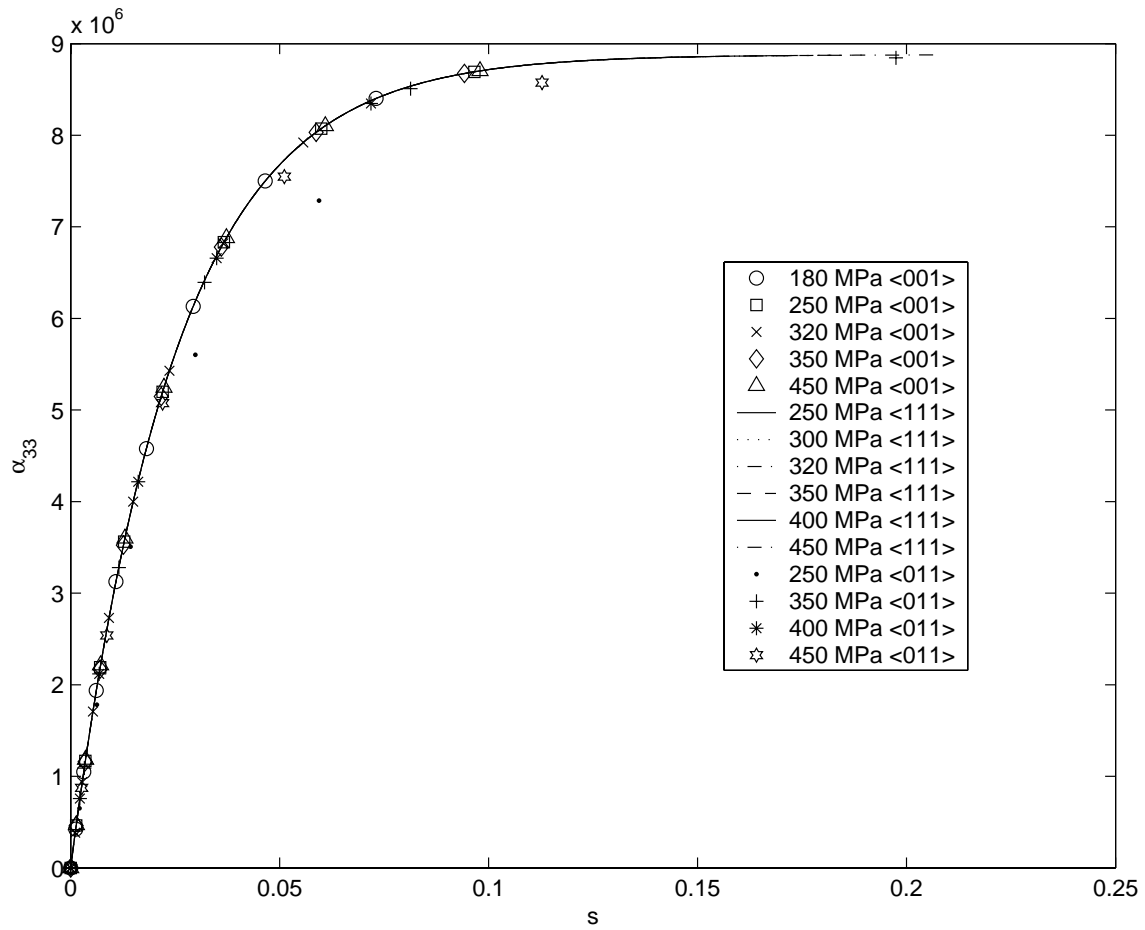
Fig. 26. Third component of backstress vs. inelastic strain pathlength for CMSX-4 , θ = 950 ^{o}C: Predictions of the model.
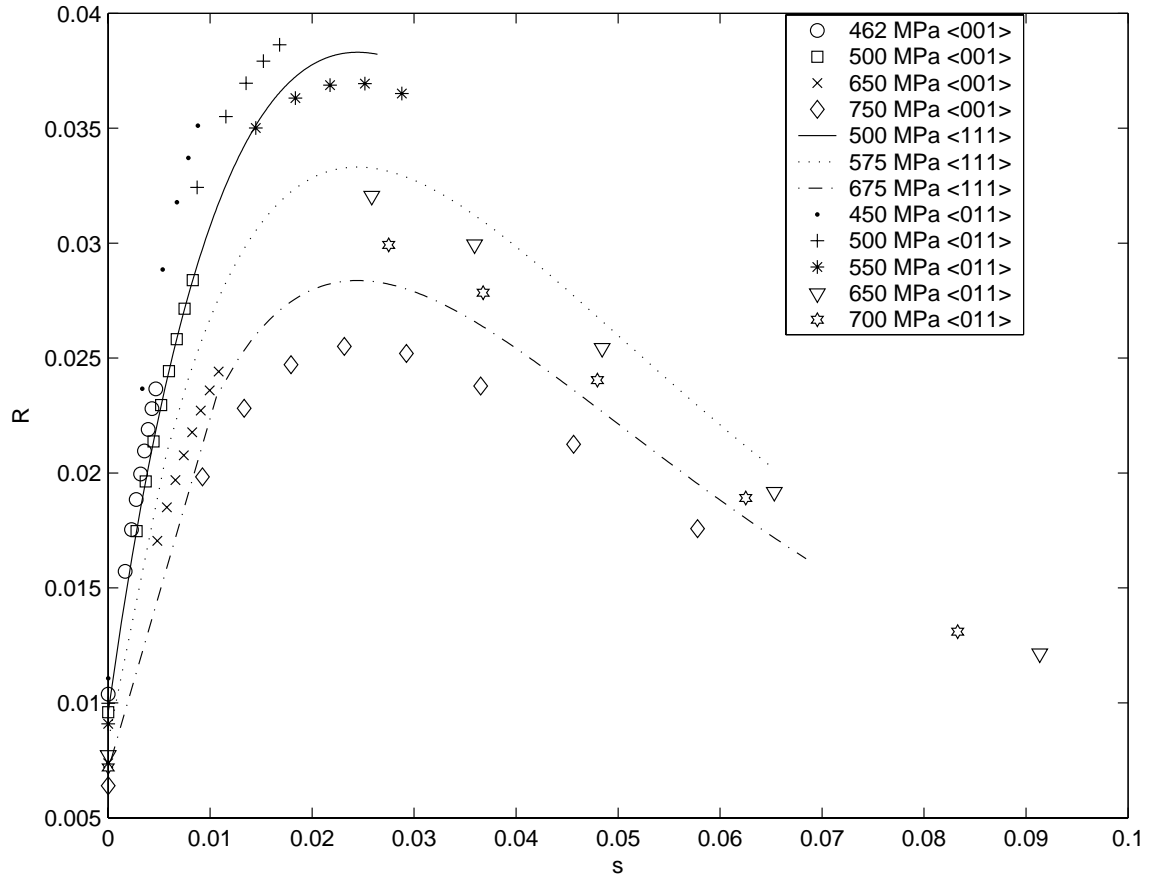
Fig. 27. Instantaneous rate of energy storage vs. inelastic strain pathlength for CMSX-4 , θ = 800 ^{o}C: Predictions of the model.
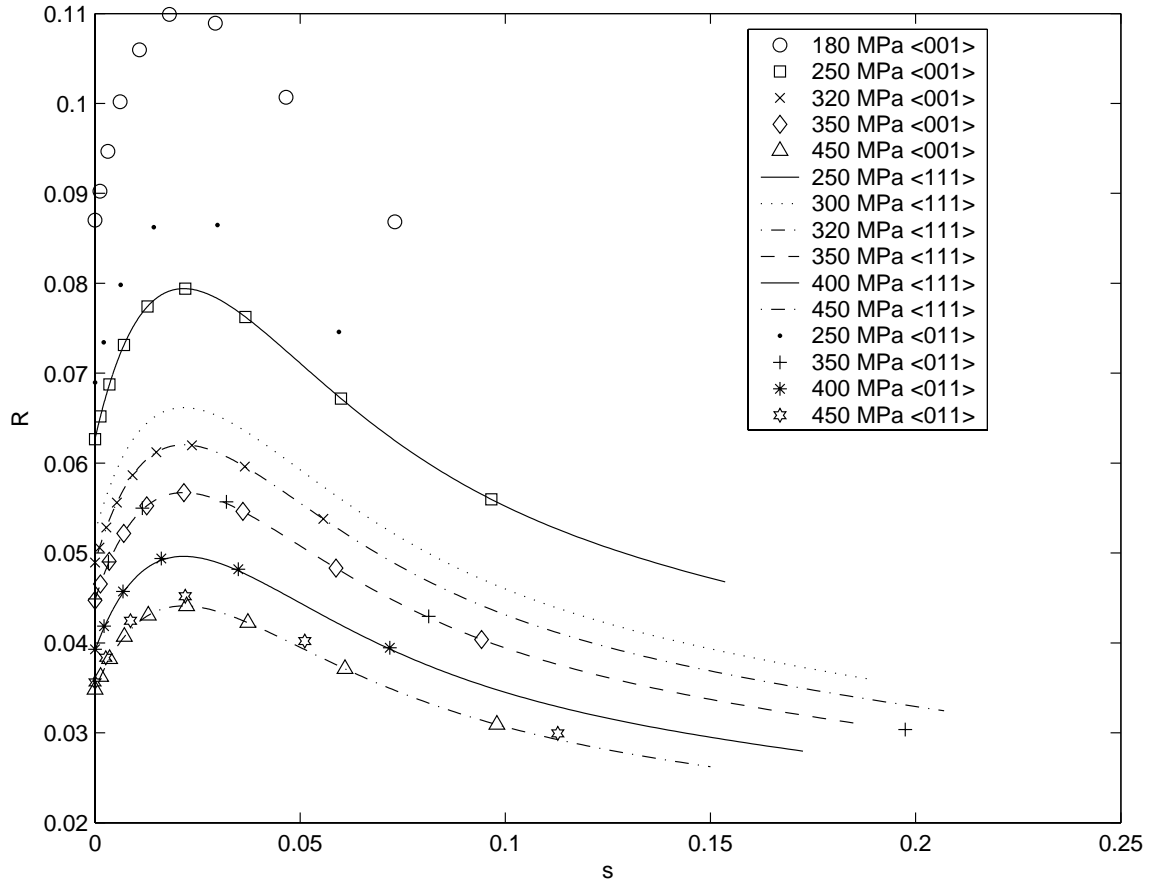
Fig. 28. Instantaneous rate of energy storage vs. inelastic strain pathlength for CMSX-4 , θ = 950 ^{o}C: Predictions of the model.
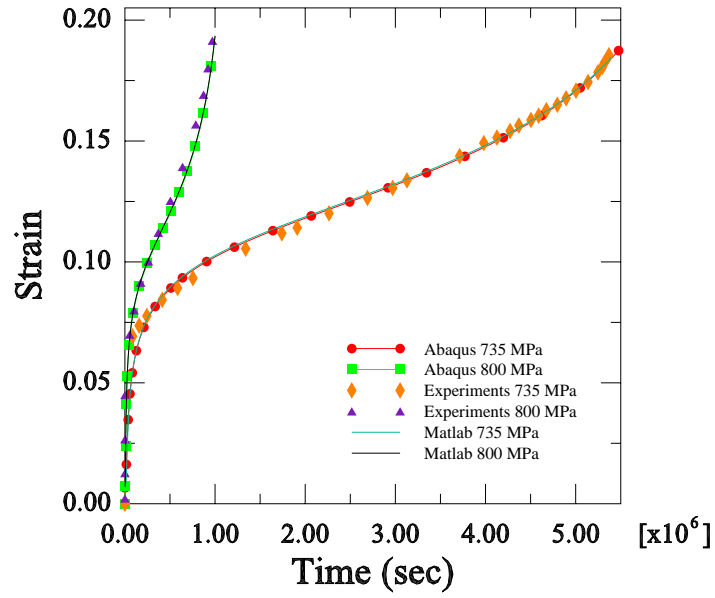
Fig. 29. Strain vs. time for CMSX-4 for loading along the <001> orientation, θ = 750 ^{o}C: Comparison of the results obtained from User Material in ABAQUS with results obtained in MATLAB and experimental results of Svoboda and Lucas [69] and Henderson and Lindblom [21].
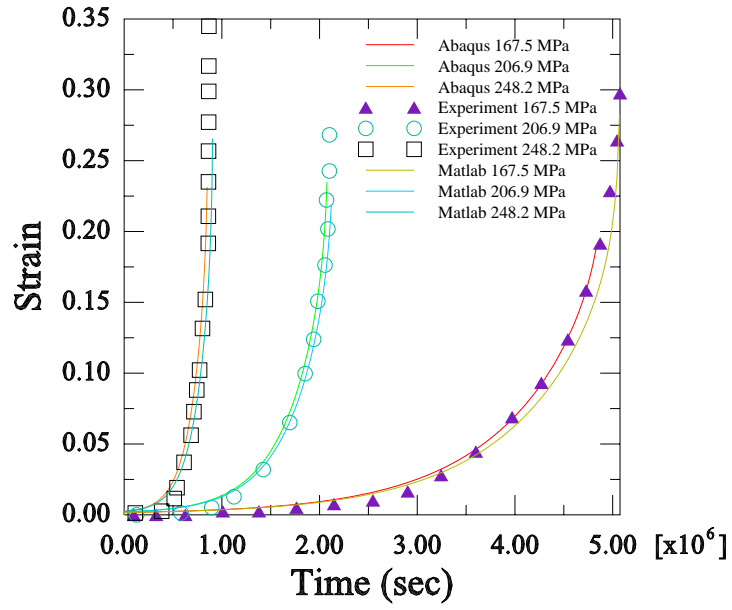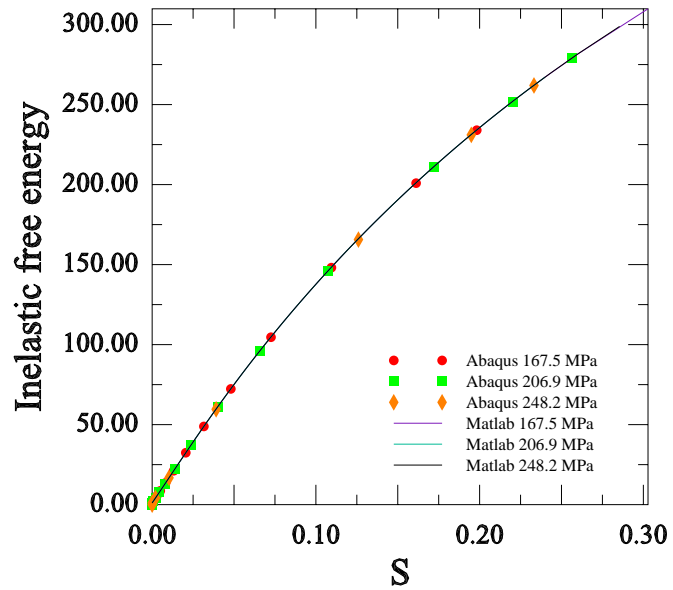
Fig. 30. Strain vs. time for CMSX-4 for loading along the <001> orientation, θ = 982 ^{o}C: Comparison of the results obtained 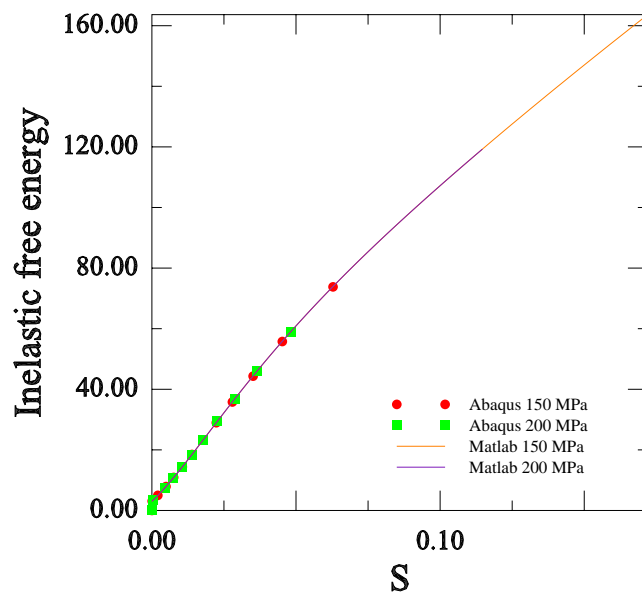from User Material in ABAQUS with results obtained in MATLAB and experimental results of Svoboda and Lucas [69] and Henderson and Lindblom [21]
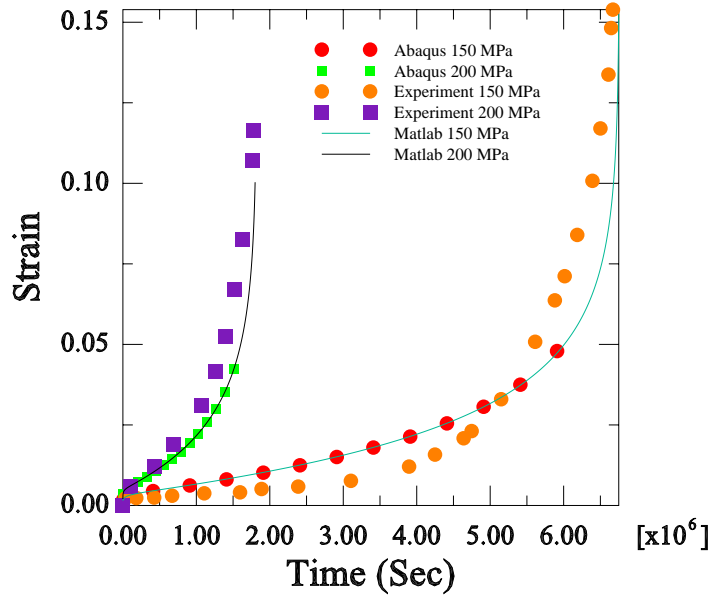
Fig. 31. Strain vs. time for CMSX-4 for loading along the <001> orientation, $\theta = 1000\ ^{o}$C: Comparison of the results obtained 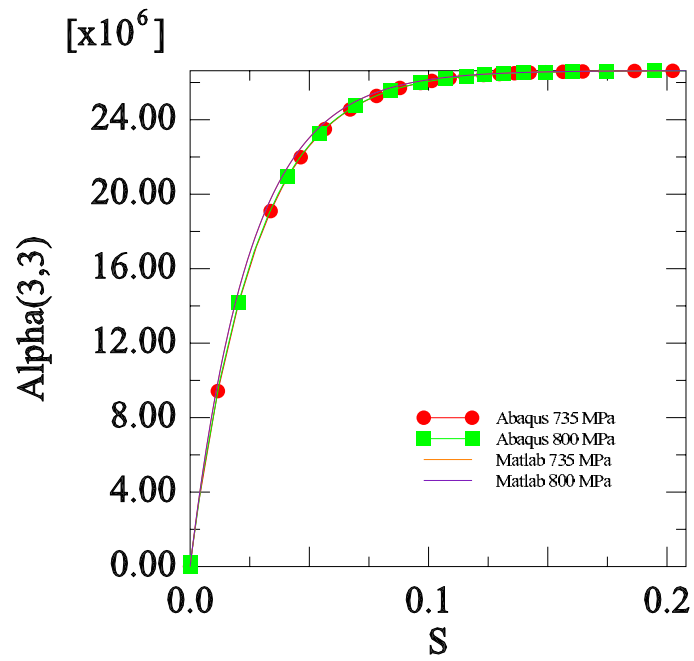from User Material in ABAQUS with results obtained in MATLAB and experimental results of Svoboda and Lucas [69] and Henderson and Lindblom [21].
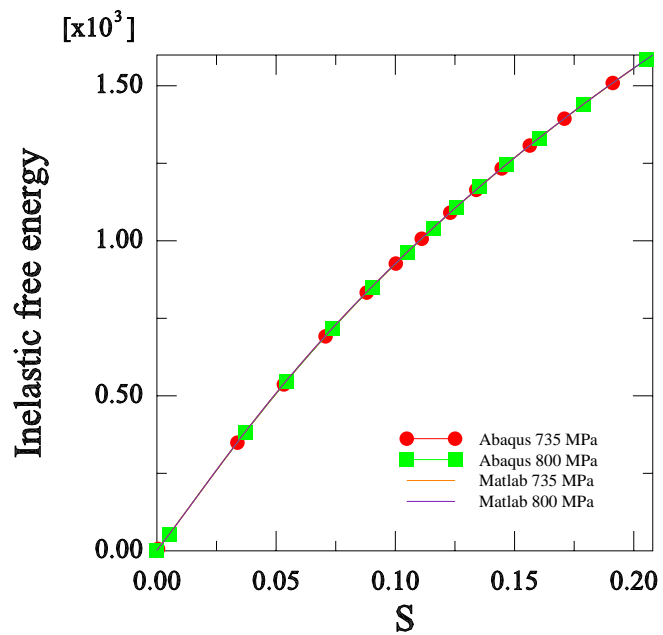
Fig. 32. Inelastic stored energy vs. inelastic strain pathlength for CMSX-4 for loading along the <001> orientation, θ = 750 ^{o}C: Comparison of the results obtained from User Material in ABAQUS with results obtained in MATLAB.

Fig. 33. Inelastic stored energy vs. inelastic strain pathlength for CMSX-4 for loading along the <001> orientation, θ = 982 ^{o}C: Comparison of the results obtained from User Material in ABAQUS with results obtained in MATLAB.

Fig. 34. Inelastic stored energy vs. inelastic strain pathlength for CMSX-4 for loading along the <001> orientation, θ = 1000 ^{o}C: Comparison of the results obtained from User Material in ABAQUS with results obtained in MATLAB.
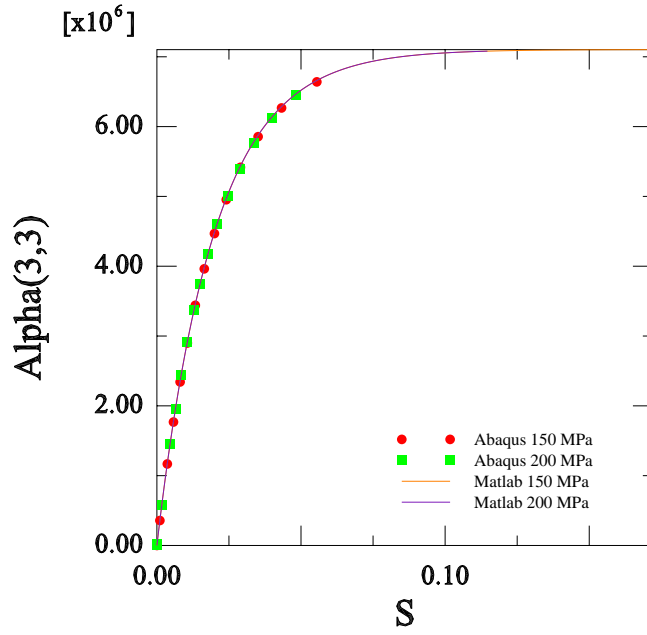
Fig. 35. Third component of backstress vs. inelastic strain pathlength for CMSX-4, $\theta = 750\ ^{o}$C: Comparison of the results obtained from User Material in ABAQUS with results obtained in MATLAB.
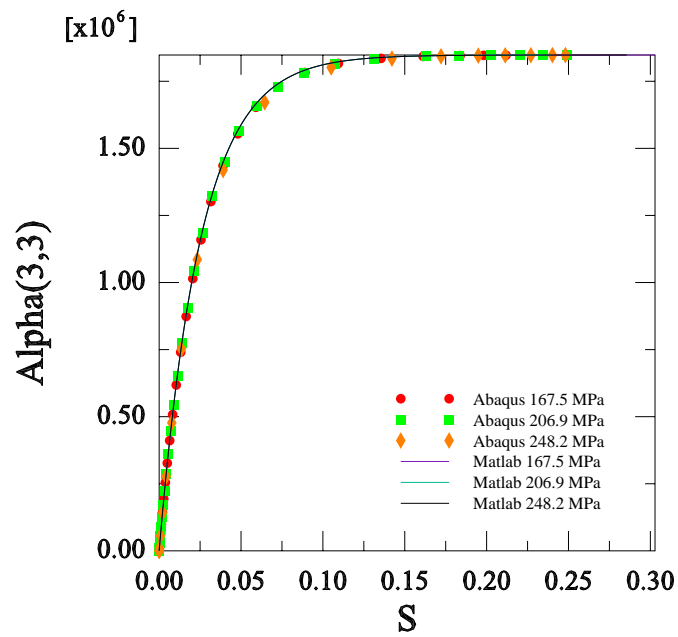
Fig. 36. Third component of backstress vs. inelastic strain pathlength for CMSX-4, θ = 982 ^{o}C: Comparison of the results obtained from User Material in ABAQUS with results obtained in MATLAB.
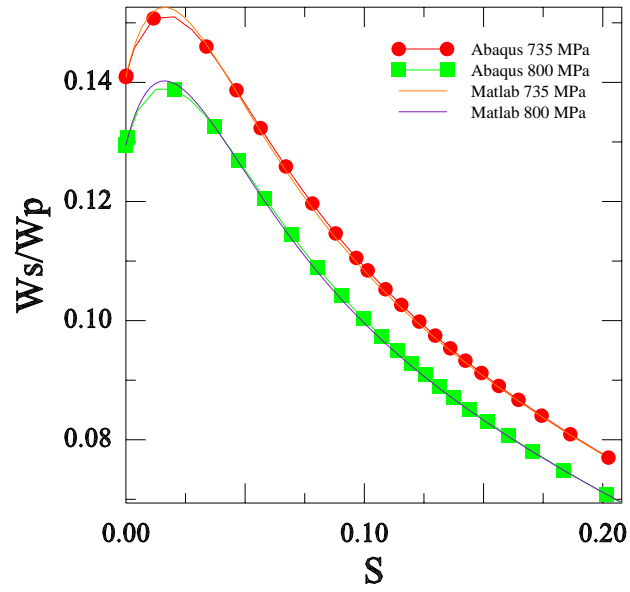
Fig. 37. Third component of backstress vs. inelastic strain pathlength for CMSX-4, $\theta = 1000\ ^{o}$C: Comparison of the results obtained from User Material in ABAQUS with results obtained in MATLAB.

Fig. 38. Instantaneous rate of energy storage vs. inelastic strain pathlength for CMSX-4 for loading along the <001> orientation, $\theta = 750\ ^oC$: Comparison of the results obtained from User Material in ABAQUS with results obtained in MATLAB.
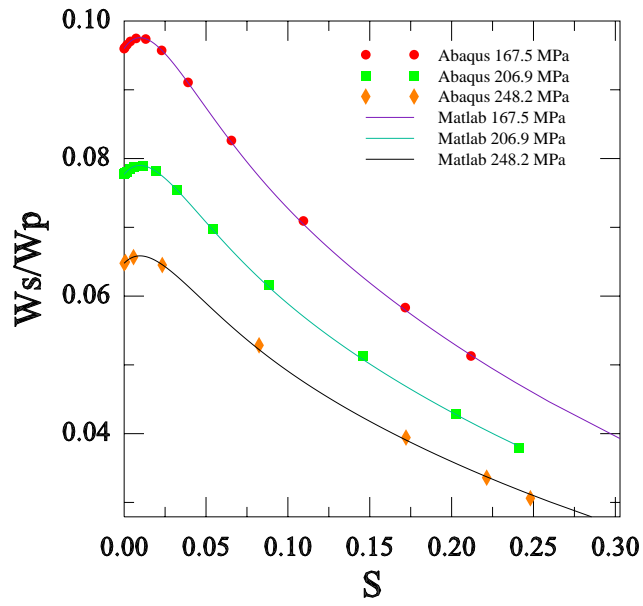
Fig. 39. Instantaneous rate of energy storage vs. inelastic strain pathlength for CMSX-4 for loading along the <001> orientation, $\theta = 982\ ^oC$: Comparison of the results obtained from User Material in ABAQUS with results obtained in MATLAB.
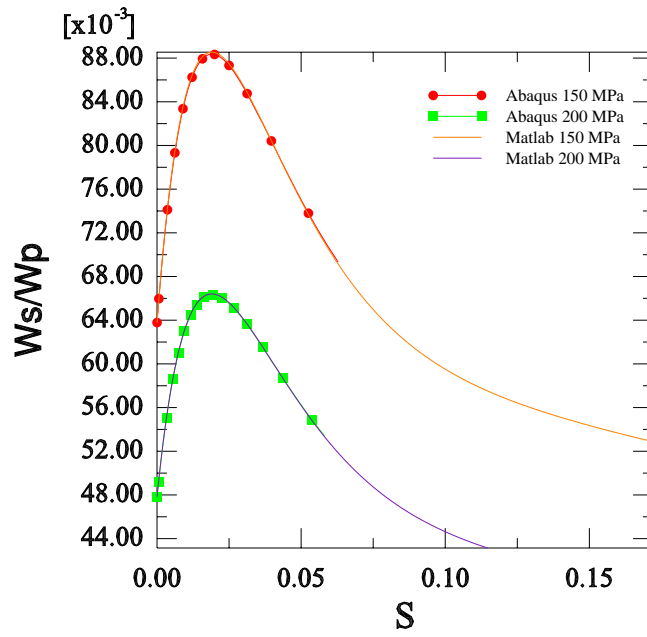
Fig. 40. Instantaneous rate of energy storage vs. inelastic strain pathlength for CMSX-4 for loading along the <001> orientation, $\theta = 1000\ ^oC$: Comparison of the results obtained from User Material in ABAQUS with results obtained in MATLAB.